THE ASTRONOMICAL JOURNAL VOLUME 106, NUMBER 6 DECEMBER 1993

A SEARCH FOR SOLAR-LIKE OSCILLATIONS IN THE STARS OF M67 WITH CCD ENSEMBLE PHOTOMETRY ON A NETWORK OF 4 m TELESCOPES

RONALD L. GILLILAND[1]
Space Telescope Science Institute,[2] 3700 San Martin Dr., Baltimore, Maryland 21218
Electronic mail: gillil@stsci.edu

TIMOTHY M. BROWN[3]
High Altitude Observatory, NCAR,[4] P.O. Box 3000, Boulder, Colorado 80307
Electronic mail: brown@hao.ucar.edu

HANS KJELDSEN[5]
European Southern Observatory, Karl-Schwarzschildstrasse 2, D-8046 Garching bei München, Germany
Electronic mail: hkjeldse@hq.eso.org

JAMES K. MCCARTHY AND MICHAL L. PERI
Palomar Observatory, California Institute of Technology, Pasadena, California 91125
Electronic mail: jkm@deimos.caltech.edu, peri@sundag.caltech.edu

JUAN ANTONIO BELMONTE[5] AND INMACULADA VIDAL[5]
Instituto de Astrofísica de Canarias, 38200 La Laguna, Tenerife, Spain
Electronic mail: jba@iac.es, ividal@iac.es

LAWRENCE E. CRAM AND JULIA PALMER
School of Physics, University of Sydney, NSW 2006, Australia
Electronic mail: lc@astrop.physics.su.oz.au, jp@astrop.physics.su.oz.au

SØREN FRANDSEN[5]
Institute of Physics and Astronomy, Aarhus University, DK-8000 Aarhus C, Denmark
Electronic mail: srf@obs.aau.dk

M. PARTHASARATHY
Indian Institute for Astrophysics, Bangalore 560034, India
Electronic mail: partha@vigyan.ernet.in

LARRY PETRO[1]
Space Telescope Science Institute,[2] 3700 San Martin Dr., Baltimore, Maryland 21218
Electronic mail: petro@stsci.edu

HARTMUT SCHNEIDER[6]
Universitäts-Sternwarte, Geismarlandstrasse 11, D-3400, Göttingen, Germany
Electronic mail: hschnei%dgogwdg1.bitnet

PETER B. STETSON[3]
Dominion Astrophysical Observatory, National Research Council of Canada, 5071 W. Saanich Rd.,
Victoria, BC V8X 4M6, Canada
Electronic mail: stetson@dao.nrc.ca

WERNER W. WEISS[6]
Institut für Astronomie, Türkenschanstr. 17, A-1180 Wien, Austria
Electronic mail: weiss@avia.una.ac.at

Received 1993 June 8

[1]Guest Observer, Kitt Peak National Observatory, National Optical Astronomical Observatories, operated by AURA, Inc. under contract with the National Science Foundation.
[2]Operated by the Association of Universities for Research in Astronomy, Inc., under contract with the National Aeronautics and Space Administration.
[3]Visiting Astronomer, Canada–France–Hawaii Telescope operated by the National Research Council of Canada, the Center National de la Recherche Scientifique de France, and the University of Hawaii.
[4]The National Center for Atmospheric Research is sponsored by the National Science Foundation.
[5]Visiting Astronomer, Nordic Optical Telescope, Observatorio del Roque de los Muchachos, Isla de la Palma, Spain.
[6]Visiting Astronomer, German Spanish Astronomical Center, Calar Alto, operated by the Max-Planck-Institut für Astronomie, Heidelberg, jointly with the Spanish National Commission for Astronomy.

 0004-6256/93/106(6)/2441/36/$0.90

ABSTRACT

Results are presented from a large observational project directed toward the detection of solar-like oscillations in an ensemble of open cluster stars. Seven groups collaborated in 1992 January to observe twelve stars in M67 with 4 m class telescopes for a one week period. High quality time series were collected on 22 telescope nights for a total of 156 h. The technique of CCD ensemble photometry allowed precisions of about 250 μmag per minute to be reached in the best cases, and provided robust results in conditions that sometimes were far from "photometric." The longitude-distributed network, coupled with generally low noise levels, provided a good window function and yielded detection thresholds of about 20 μmag (five times solar) for solar-like oscillations in the best ensemble stars. Sensitivity to solar-like oscillations over our twelve ensemble stars ranges from 30% to a factor of three better than obtained previously by any group. When our simultaneous results for 12 stars (prior most sensitive result followed from photoelectric photometry on a single star) is taken into account this project provides a (multiplexed) factor of 20 to 30 gain over previous experiments. For two stars we derive interesting upper limits for oscillation amplitudes that are near the lower range predicted by theory. Over half the stars in the ensemble show suggestive evidence for oscillations; we develop the evidence for, and the cautions against, claiming detections in these cases. Given the unique aspects of this project we describe in detail the observation planning process, data acquisition, reductions, and ensuing analyses. We argue that a more aggressive network campaign could provide a factor of two sensitivity gain with a resulting high probability of attaining unambiguous oscillation detections on most of the stars in the M67 ensemble.

1. INTRODUCTION

Several of the team members have been pursuing means of detecting solar-like *p*-mode oscillations on other stars via both spectroscopic and photometric means. The nature of solar oscillations and their expected stellar analogues place severe constraints on observations directed at their detection. The Sun observed as a star, i.e., without spatial resolution, shows many modes of angular degree $l=0$, 1, and 2 and different radial orders, $n\approx 15$ to 25. The solar modes have amplitudes of at most ~ 20 cm s^{-1} in velocity and ~ 4–10×10^{-6} in relative broadband intensity [the lower value follows from analysis of Fröhlich (1991) and Toutain & Fröhlich (1992), while the higher range is from Jiménez *et al.* (1990)]. Existing theory by Christensen-Dalsgaard & Frandsen (1983) suggests that stars somewhat hotter and more evolved than the Sun may have peak amplitudes a few times larger.

Even selecting roughly solar-like stars with favorable predictions for oscillation amplitudes, we are searching for modes with very small amplitudes, perhaps 1 m s^{-1} or 20–50 μmags. The solar modes have peak amplitudes near periods of about 5 min; stars chosen for prediction of larger amplitudes are expected to have periods a few times longer.

An outstanding observational aspect of solar oscillations is that different modes occur at regular frequency intervals, providing a "picket-fence" effect in power spectra. This property reflects the convenient theoretical representation of mode frequency spacings in terms of a simple asymptotic formula. This asymptotic relation (see, e.g., Vandakurov 1968; Tassoul 1980; Christensen-Dalsgaard 1988) is generally valid for $n/l \gg 1$ (satisfied for the Sun and expected to hold for the stars of primary interest in this paper) and gives individual mode frequencies as

$$\nu_{n,l}=\Delta\nu_0(n+l/2+\epsilon)-Al(l+1)/(n+l/2+\epsilon), \quad (1)$$

where ϵ is a parameter of order unity relating primarily to the star's near-surface structure and A relates more sensitively to conditions near the stellar core. For our purposes (obtaining observations to unambiguously detect stellar oscillations), it is sufficient for now to recognize that the first feature likely to be noticeable in power spectra is $\Delta\nu_0/2$, roughly the separation between $\nu_{n,1}$ and $\nu_{n+1,0}$. A measurement of $\Delta\nu_0$ provides a tight constraint on the stellar radius via

$$\Delta\nu_0 \propto \mathcal{M}^{1/2}R^{-3/2}, \quad (2)$$

where $\mathcal{M}$ is the stellar mass and R is the radius. This mean density relationship holds for stars that are strictly homologous (Cox 1980), but also works well for stars not obeying such simple scaling (Ulrich 1986). $\Delta\nu_0/2$ is proportional to the inverse sound crossing time; in the Sun it takes a value of 68 μHz. Stars selected (for their favorable amplitude predictions) to be somewhat hotter and more evolved than the Sun have larger radii and hence a smaller value of $\Delta\nu_0/2$, about 30 μHz for the stars we discuss further below. Separations of 30 μHz are quite awkward to detect: for reasons discussed further in Secs. 2 and 5, observations from a single site are incapable of resolving 30 μHz splittings using the simplest analysis techniques. To have a good chance of detecting the stellar analogue of solar oscillations, a longitude-distributed network of coordinated observing is required.

The second-order coefficient, A, represents the breaking of degeneracy between modes with $l=0$ and 2 and may be represented observationally as

$$\Delta\nu_{20}=\nu_{n,0}-\nu_{n-1,2}. \quad (3)$$

The quantity $\Delta\nu_{20}$ has a value of 9 μHz for the Sun. The "small separation" $\Delta\nu_{20}$ arises from the structure of the star in regions that are sampled differently by modes with $l=0$ and $l=2$, i.e., the stellar core. This frequency separa-

tion is therefore sensitive to the evolutionary state of the star (Christensen-Dalsgaard 1988).

To emphasize how small the solar amplitudes are in a practical sense, consider how many intensity measurements at a relative precision of 10^{-3} would be needed to reach a noise level of 10^{-6} required for a quantitatively useful (but fairly noisy) detection. To bridge the three orders of magnitude between one observation and the desired overall precision requires 10^6 observations. Indeed it was observations with roughly these characteristics (many months worth of 2.2 min integrations) obtained with the ACRIM solar irradiance monitor on the SMM spacecraft (Woodard & Hudson 1983) that first detected solar oscillations photometrically. Gilliland & Brown (1988) demonstrated CCD ensemble photometric precisions of about 10^{-3} per minute on 1 m telescopes. Such precision levels would have to be maintained for three years to detect a perfect solar analogue. Although we can expect the number of required observations to drop in proportion to improved per integration precision, and as the square of limiting precision required for larger amplitude oscillations, the photometric detection of solar-like oscillations remains a daunting prospect.

Given the extreme difficulty of detecting stellar oscillations, is their pursuit worthwhile? We believe so, for the following reasons. The detection and subsequent quantitative study of solar p modes over the past two decades has revitalized the field of solar physics; for the first time astronomy has an effective probe into the inner conditions of an ordinary star. It is then natural to suppose that more might be learned by application of similar principles to stars other than the Sun. Detection of solar analogue oscillations will likely improve existing structural information about individual stars. Unambiguous detection of oscillations on many related stars (as in an open cluster) is even more exciting, however, since it holds the promise of providing fundamentally new tests of stellar structure and evolution theory. In a general sense, knowledge of five adjustable parameters (mass, age, metallicity, initial helium abundance, and a mixing length parameter) is considered sufficient to uniquely describe the structure of ordinary stars. Knowledge of a like number of independent observables may be used to test the predictions of theory. Detection of stellar oscillation frequencies would provide an additional pair of basic observables for each star observed. For an ensemble of cluster stars all having the same age and abundance parameters, a relative comparison of photometric and spectroscopic data with the addition of oscillation frequencies should provide more observational constraints than the number of simply adjustable parameters. The potential then exists to obtain observational overdetermination for an ensemble of cluster stars, and thus allow testing of basic assumptions and fine details of stellar evolution theory (see Brown 1991 for a more complete discussion).

The combination of great promise for stellar astrophysics coupled with the great practical difficulties of observational asteroseismology has led to a large number of excellent review papers discussing the theory and prospects, while the number of unambiguous detections for solar-like stars remains at one: the Sun itself. Recent reviews of helio- and asteroseismology include: Libbrecht & Woodard (1991), Brown (1991), and Gough & Toomre (1991). This large investment of planning for what may be learned from asteroseismology, relative to current results, is necessitated by the large commitment of community resources [either via spacecraft, see Appourchaux *et al.* (1991), or large telescope time] that will be required for observational success.

In Sec. 2 of this paper we will discuss our choice of a stellar ensemble to observe, and the substantial planning effort preceding the observations. Section 3 provides details of the observations acquired at each of the collaborating sites. Aspects of calibrations, CCD reductions, and analysis techniques that are unique to this project will be explored in Sec. 4. An outline of the techniques used to search for oscillations in our low signal-to-noise ratio data, a development of upper limits to allowed amplitudes and a comparison of precisions with previous photometric studies are the topics of Sec. 5. In Sec. 6 we develop, on a star-by-star basis, the best evidence for oscillations, and also provide significance estimates. In Sec. 7 we explore the future prospects for projects aimed at asteroseismology based on ground-based photometry. The reader may find it useful to skip ahead to the discussion and summary provided in Sec. 8 before reading the more detailed sections.

2. PLANNING THE OBSERVATIONS

Realizing that a project of this scope cannot be repeated often, we put a great deal of effort into the field selection, telescope time applications, and detailed planning for observations at each site. Part of the inducement for telescope allocation committees to grant substantial 4 m time to this admittedly risky project was that we were planning this as an isolated, "all out" effort, and that we would not reapply for a similar effort for a few years. In a network campaign for which intense observational coverage is required, the whole is truly greater than the simple sum of the parts.

2.1 Selection of Stellar Ensemble

We will begin by enumerating some rather obvious properties of an ideal stellar ensemble for high precision CCD photometry. Next we will present the object list for the region of the sky selected, and finally justify that it was, in fact, *the* best field to observe for this project. The interpretive value of observed stellar oscillation frequency splittings increases dramatically as knowledge of fundamental stellar parameters (like mass, age, and composition) improve (Gough 1987; Brown 1991). This argues for selection of an open cluster for which a full suite of comprehensive astronomical investigations (precise absolute photometry, proper motions, spectroscopy to define compositions, binarity searches, isochrone fitting, etc.) have already been performed. (Clusters satisfying this requirement include the Hyades, Pleiades, NGC 188, NGC 752, M67, and perhaps a few others). We (Gilliland & Brown 1992 and Kjeldsen & Frandsen 1992, hereafter referred to

as GB92 and KF92, respectively) have experience with CCD ensemble photometry showing that atmospheric transparency variations could be effectively removed with fields spanning 3–4 arcmin within the precision allowed by 2 m class telescopes. With 4 m class telescopes for which better precision was anticipated, we wished to err on the side of conservatism and restrict candidate fields to strictly less than 3 arcmin, for which we expected atmospheric transparency fluctuations to remain coherent. This immediately ruled out nearby clusters like the Hyades and Pleiades which span much larger fields. Along these same lines we were also forced to consider what CCD fields of view were readily available at 4 m telescopes; typically RCA 320×512 (30 μ pixels) and TEK 512×512 (27 μ pixels) devices mountable at $\sim f/4$ or $f/8$ were available in early 1992. This limited the field of view (FOV) to ~90 to 180 arcsec. At Kitt Peak the excellent AR coated TEK 512 (T5HA, which remains the best CCD available for these observations) spans 92 arcsec if mounted at the $f/8$ Ritchey–Chrétian focus, or 276 arcsec if mounted at the $f/2.7$ prime focus. The larger image scale (0.18 arcsec per pixel) at $f/8$ was advantageous, allowing the large per readout dynamic range as further discussed in the next section. Also this smaller FOV could be spanned by essentially any other 4 m site, while an ensemble matched to 276 arcsec could be a problem at some other sites. Therefore, given a nominal Kitt Peak 4 m FOV of 92 arcsec and experience with the well studied solar-age open cluster M67, we searched for optimal fields in that cluster. The ideal field would have at least 10 stars of the desired spectral type (Sun-like in a loose sense), few or no contaminating brighter or fainter stars, and a good clear region from which the sky background could be determined. As discussed in Sec. *2.3* the ensemble stars should also be separated from each other by a least three times the expected usable seeing conditions; taking 4 arcsec as a reasonable cutoff this implied desired separations of $\geqslant$12 arcsec. To assure that errors from Poisson statistics with 4 m telescopes do not greatly exceed the contribution from atmospheric scintillation (averaged over full-night windows) required stars in the range of $B\sim$13th magnitude, or preferably brighter.

The field selected is the "dipper asterism" region in M67; it is displayed in Fig. 1 and detailed in Table 1 (taken largely from GB92). This is clearly the field within M67 best satisfying the general selection criteria. The only real weakness of this field is that it is a little faint; it does not provide results limited by atmospheric scintillation on 4 m telescopes, which would require stars of $B\sim$11th magnitude for which the Poisson contribution would be unimportant (GB92; KF92). However, as discussed further in Sec. *2.3*, brighter stars would have been problematic for some sites. The selected field is ideal in that all stars are high probability cluster members (Girard *et al.* 1989), are well studied photometrically (e.g., Nissen *et al.* 1987; Gilliland *et al.* 1991, hereafter referred to as G91), spectroscopically (Mathieu *et al.* 1990; Pritchet & Glaspey 1991; Hobbs & Thorburn 1991), astrometrically (Girard *et al.* 1989), and theoretically (Morgan & Eggleton 1978; De-

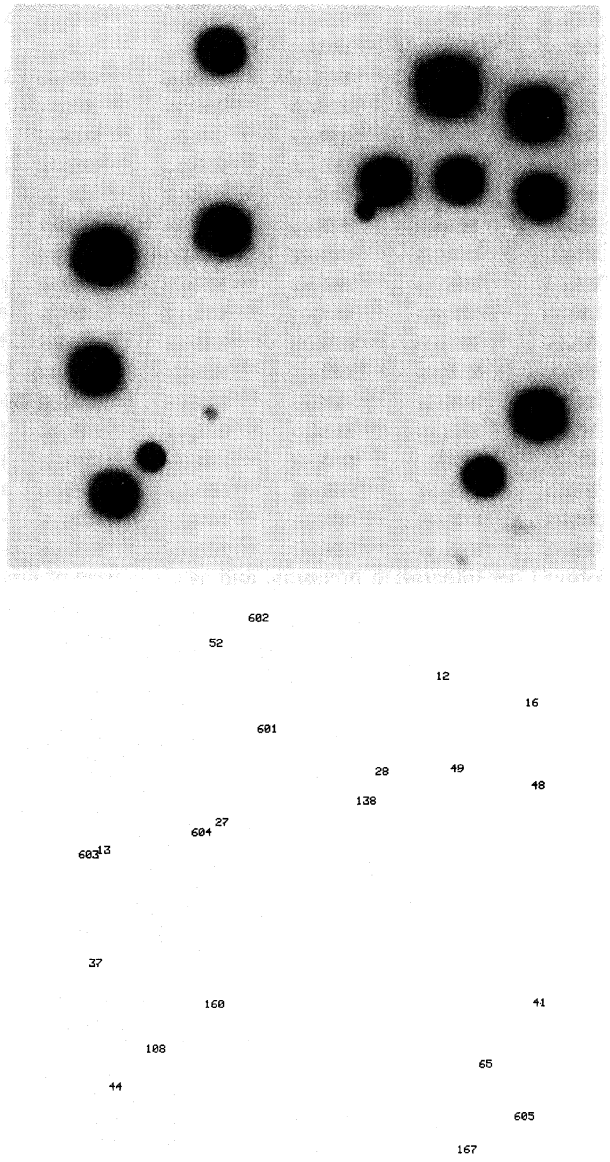

FIG. 1. M67 "dipper asterism" field selected for stellar oscillations campaign. Upper box shows one CCD frame taken with the Kitt Peak 4 m with a 92″ FOV. Lower box provides identification numbers for stars (see also Table 1).

marque *et al.* 1992; GB92), and span a relatively small range of magnitudes and color. The stellar types map out an interesting region of the HR diagram surrounding the main-sequence termination. Of vital importance to the project justification was that oscillation amplitudes for several of the stars were projected to be three to five times solar levels, making their detection feasible.

In Table 1 the star numbers are from GB91 with cross references to Sanders (1977), Fagerholm (1906), and Eggen & Sandage (1964). Columns for m_V, $B-V$, $T_{\rm eff}$, $L/L_\odot$, $\mathcal{M}/\mathcal{M}_\odot$, $\Delta\nu_0/2$, and $\Delta\nu_{20}$ are taken directly from GB92. All frequencies are in μHz. The expected amplitude column (Amp in parts per million, ppm) has been revised

TABLE 1. M67 stellar ensemble properties.

No.	m_V	$B-V$	$T_{\rm eff}$	$L/L_\odot$	$M/M_\odot$	$\Delta\nu_0/2$	$\Delta\nu_{20}$	$\nu_{\rm pk}$	Amp	Sens	Cross-ref
12	11.45	1.09	4550	19.2	1.360			96	76-173	15	989, F135
13	12.14	0.46	6520	8.6	1.600	26.1	4.6	885	18-41	15	997, F124
16	12.27	0.59	6050	7.7	1.280	28.7	5.1	608	23-52	16	984, F134
27	12.78	0.57	6120	4.8	1.280	28.8	5.1	1016	17-38	18	995, F127
28	12.91	0.46	6520	4.2	1.375	42.1	8.2	1557	12-27	18	2204, F130
37	12.63	0.80	5170	4.3	1.340	17.3	3.4	658	23-52	18	999, F117
41	12.73	0.57	6120	4.7	1.280	28.8	5.1	1038	16-37	18	986, F111
44	13.09	0.56	6160	3.6	1.265	36.3	6.0	1370	13-31	20	998, I-11
48	13.16	0.58	6085	3.4	1.255	37.6	6.2	1378	13-31	20	2205, I-198
49	13.20	0.58	6085	3.3	1.245	38.9	6.4	1409	13-30	20	988, I-199
52	13.22	0.58	6085	3.2	1.235	40.2	6.6	1441	13-30	20	994, I-9
65	13.94	0.60	6010	1.7	1.105	56.1	8.9	2324	8-17	28	987, I-226
108	15.80	1.09									I-10
138	17.78	1.51									I-224
160	19.50	0.93									I-246
167	19.81	1.51									I-225
601	21.91	1.50									
602	22.32	0.00									
603	16.46	0.89									
604	19.46	1.30									
605	19.24	1.50									

(no significant differences on average) using the theory of Christensen-Dalsgaard & Frandsen (1983) and the derived scaling law

$$\mathrm{Amp}/\mathrm{Amp}_\odot = 2[(g/g_\odot)^{0.6} + (g/g_\odot)^{4.5}]^{-1}, \quad (4)$$

where g is the surface gravity, from Kjeldsen (1993a). The value ν_{pk} shows the expected frequency of maximum p-mode oscillation amplitudes based on a simple scaling from the Sun. The solar p modes lie between 1.5 and 4.5 mHz, peaking near 3 mHz. This frequency range is thought to be determined by the stellar atmosphere acoustic cutoff frequency

$$\nu_{\rm ac} \propto g T_{\rm eff}^{-1/2}, \quad (5)$$

where g is the surface gravity and $T_{\rm eff}$ is the effective temperature. For the Sun $\nu_{\rm ac} \approx 5.5$ mHz or 1.8 times the frequency at which oscillations peak. We simply assume the same ratio of maximum power to acoustic cutoff frequency to define $\nu_{\rm pk}$; this should be taken as a rough guide to where the oscillations are likely, not as a firm constraint. The sensitivity values were evaluated as Sens $= 2\sigma(\mathrm{SN}/N_{\rm obs})^{1/2}$ (Scargle 1982), where Sens is the coherent amplitude detection threshold, σ is the time series rms, SN is the desired signal-to-noise level for detection and $N_{\rm obs}$ is the number of observations. With a SN of 4 these are the numbers we projected for a successful 4 m network campaign, and are the numbers in several of our telescope time applications. This value of Sens also corresponds to the level of 4σ deviant peaks in a power spectrum of white noise. Objects 108 through 605 are included for completeness, but are not considered an integral part of the ensemble. The objects starting with 601 were first detected with the 4 m M67 time series data; magnitudes are rough estimates relative to the ensemble stars with colors derived by calibrating against the dependence of count rate on airmass.

It is not possible to give reliable error estimates for all of the entries in Table 1. However, we can provide a general estimate of likely errors. For a star like No. 27 with an HR diagram position easily matched by the standard 4.0×10^9 yr isochrone (GB92) errors of $T_{\rm eff}\pm200$, $L/L_\odot\pm10\%$, $\mathcal{M}/\mathcal{M}_\odot\pm0.03$, and $\Delta\nu_0/2\pm10\%$ are reasonable estimates. For a star like No. 16 with an anomalous HR diagram position the interpretation becomes uncertain at a much larger level; in Sec. *6.1* we will argue that a consistent interpretation of No. 16 as a single star yields $\Delta\nu_0/2\sim20\ \mu$Hz. Further discussion of confidence levels on individual stars will be provided in Sec. 6.

An object visible in January was desired for two reasons. Given that most 4 m telescopes are in the northern hemisphere, selection of a winter target would provide full 9 h observing windows at each site. For a strictly pragmatic reason related to organizing the network, M67, which in mid-January rises two hours after sunset, was also seen as ideal. With the Kitt Peak proposal semester running August through January with an application due in March we would know the outcome of the Kitt Peak application before the submission deadline for many other sites. Time on the Kitt Peak 4 m was requested to "anchor" the project and then with this in hand we could better justify the campaign to other sites.

Having settled on the time of year to observe (mid-January) and the field of view ($\sim$90 arcsec) we then performed a search of the 4000 square degree region of sky that could be observed, listing all 90″ fields from the space telescope *Guide Star Catalogue* (Lasker *et al.* 1990) containing 10 or more stars brighter than $m_V=14$. Only two such fields turned up, one of which was the already nominally selected dipper asterism in M67, and on balance this field was superior on a number of counts. We therefore feel confident that given our general constraints, the M67 field

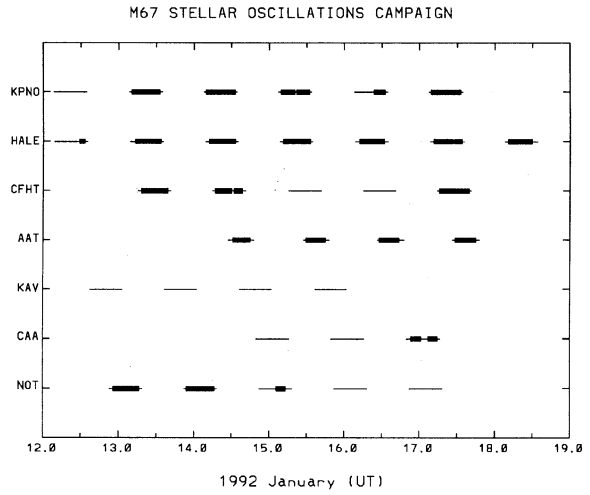

FIG. 2. Light lines show allocations of time with airmass $\leqslant 3$. Thick lines show periods for which time series of good quality were obtained on M67. From the top the sites and observers were: KPNO (Kitt Peak 4 m, R. L. G. and L. P.), HALE (Palomar 5 m, J. K. M. and M. L. P.), CFHT (Canada–France–Hawaii 3.6 m, P. B. S. and T. M. B.), AAT (Anglo–Australian Telescope 3.9 m, L. E. C. and J. P.), KAV (Kavalur 2.3 m, M. P.), CAA (Calar Alto 3.6 m H.S. and W. W. W.), and NOT (Nordic Optical Telescope 2.5 m, S. F., H. K., J. A. B., and I. V.).

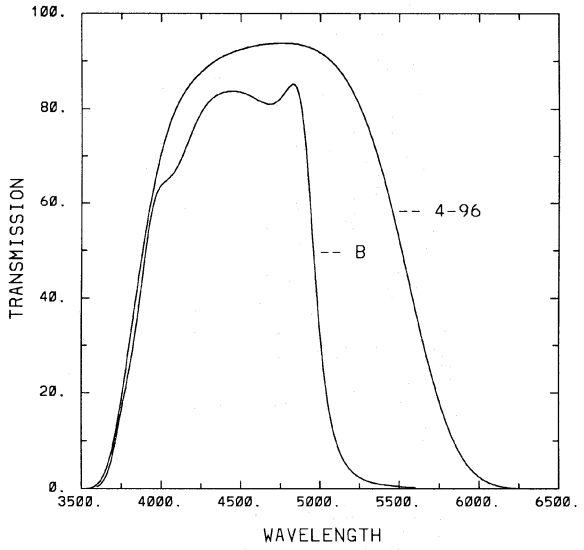

FIG. 3. Tracing (provided by Ed Carder of NOAO) of AR coated Corning 4-96 filter. Kitt Peak "nearly Mould B" tracing is shown for comparison.

was not only an excellent choice, but the best candidate for the current project.

2.2 Constraints Set by Oscillation Properties

Taking the entries in Table 1 as a guide to the signals we were seeking, how did this drive the network formation? The simulations shown as Figs. 6 and 7 of GB92 were central to this issue. In Fig. 6 (GB92) we showed a simulation for star No. 27 in which data would be obtained over 16 h windows for six nights at precisions (250 μmag every 2 min) expected from 4 m class telescopes; in this case a simulated signal at 40 μmag peak amplitude is clear and quantifiable with multiple analysis tools (CLEANed power spectrum, power spectrum of power spectrum and a folded power spectrum). An identical simulation, but with the same total data placed in 8 h windows, such as could be obtained with multiple sites at one longitude (or a single 8 to 10 m telescope), failed to show good evidence for the imposed signal.

To have good sensitivity to oscillations for the stars (Nos 13–41 of Table 1) with favorable amplitude projections and primary frequency separations of typically ~ 28 μHz, one needs nightly windows of $\sim 1.5/28$ μHz$=15$ h. If the observing windows are much under 15 h sensitivity to the critical frequency spacing detection is compromised. Nightly windows better than 15 h are desirable, but not of primary importance.

The sensitivities listed in Table 1 assumed 96 h of excellent data with a noise level that could only be obtained with 4 m class telescopes. With 16 h windows (two independent longitude sites each night) this requires six nights. With typical winter conditions limiting good nights to perhaps 50% of the total awarded, it seemed imperative to have at least four 4 m telescopes assigned to the project for about six nights each. Also consistent with this length of run is the time required to safely resolve the smallest $\Delta\nu_{20}$ (star 37) frequency. This implies 1.5/3.4 μHz$=5.1$ days.

Assuming that we might not be successful in all cases, a total of nine telescope applications were submitted, of which seven were successful. Figure 2 illustrates the telescope time granted to this project, as well as the fraction of time during which observations were actually obtained. Details of the observations will follow in Sec. 3.

A far greater challenge than gaining access to 30+ nights of 4 m class telescope time was assuring that each site would provide near optimal data, limited only by atmospheric scintillation and Poisson statistics. This concern was compounded by the fact that most sites would be operated by observers interested in the science, but with little experience in limiting precision CCD photometry. Further complicating this was the case (except for the NOT) that the telescope–instrument–observer combination was without experience at each site. Developing the techniques to optimize the quality of CCD frames accumulating at one per minute for a new project is not to be recommended as a real-time exercise on 4 m telescopes, so we took unusual steps to meticulously preplan the observations at each site.

2.3 Optimizing Setup at Each Site

Recognizing that our ensemble stars were marginally fainter than optimal, we decided upon use of a broad filter with high overall efficiency. We wished to avoid regions blueward of 3800 Å and redward of 5800 Å to minimize the impact of atmospheric variations. After reviewing existing Kitt Peak broadband filters, we selected a Corning glass filter, 4-96 5 mm thick with a central wavelength of 4720 Å, a FWHM of 1665 Å and a peak (AR coated)

throughput of 93.8%. This filter matched very closely our general desires and one was ordered for each site (except NOT, which opted to use the blue channel of an available beam splitter giving a similar total system response). Figure 3 shows a tracing of the AR coated Corning 4-96 filter. With typical CCD response and stellar flux versus wavelength factored in the 4-96 filter provides a count rate 2.5 times that of a standard *B* filter.

To illustrate the setup problems at different sites let us consider the integration times initially estimated for two sites: KPNO and CFHT. Based on knowledge of the filter and direct experience with the chosen TEK CCD on other Kitt Peak telescopes, we could easily predict a count rate for the brightest ensemble star of about $8\times10^5 e^-$ s^{-1}. With assumed 1.5″ seeing and a pixel scale of 0.18″/pixel, about 1% of the total light would hit the central point spread function (PSF) pixel (based on empirical knowledge of PSF shapes). With a full well (and known to be linear) depth of $5.5\times10^5 e^-$ we could thus integrate for ~68 s before saturation occurred. Keeping to ~50 s integrations to avoid saturation and with a CCD readout overhead time of 20 s we could maintain a favorable duty cycle of 71%. One minute integrations also provided about the right sampling frequency for our stars. At CFHT we were to use the 15μ pixel RCA4 with a linear range of only $6\times10^4 e^-$. We were forced to use the prime instead of the more desirable Cassegrain focus, yielding an image scale of 0.2″ per pixel. At CFHT seeing of 0.6″ does occur, putting some 4% of the PSF intensity on the peak pixel. With a very similar predicted count rate for the brightest stars as at the KPNO 4 m, 75% of CCD saturation would occur in ~1.8 s. With a CCD cycling time of perhaps 16 s, this yields an abysmal duty cycle of ~10%. Since both Poisson noise and atmospheric scintillation scale as the inverse square root of duty cycle, this would yield errors for CFHT nearly a factor of three higher than for Kitt Peak. The solution for CFHT was obvious: defocus the telescope so that more photons could be counted per integration, allowing a good duty cycle of 60%–70% to be reached. But how much defocus should be used? We are trying to measure individual star intensities at a precision where 1 part in 10^4 matters. With substantial defocus, and/or poor seeing, images begin to blur together and the ability to recover individual star intensities to the requisite precision can be compromised.

The goal at each site was simple: with the equipment at hand (differing widely from site to site) and the existing conditions (primarily seeing), obtain the data in such a way as to provide the best sensitivity to oscillations detection. As a function of imposed seeing, what combination of exposure time and telescope defocus should be adopted? This is a multidimensional minimization problem which we solved separately for each site.

A simple FORTRAN code was developed to treat all sites. Input data included telescope aperture, latitude and altitude, CCD pixel scale, saturation level, readout noise and overhead time, as well as the total system efficiency and assumed sky brightness. The code included time dependent estimates for Poisson statistics, taking into account a nominal extinction versus airmass function and atmospheric scintillation. An error term depending on both seeing and defocus was included, based on the known empirical effect of the two effects on the PSF. This defocus plus seeing penalty term was set to 20% of the relative intensity contributed to one star in an area containing 99% encircled energy by a neighbor of equal intensity 11″ away (approximately the minimum separations in our ensemble). Previous experience suggested that optimal digital aperture sizes corresponded to 99% encircled energy. The penalty term is set to only 20% of the nominal contamination level, since it is only the *variation* over time of the contamination that matters for differential photometry. At a seeing of 3.5″ with a 99% encircled energy radius of 10.3″, we estimate the direct contamination from an 11″ companion of equal intensity to be 1.4%. With 20% of this remaining as noise from uncompensated seeing fluctuations there would be an additional error term of 2800 μmag—many times larger than our goal. The problem is of course not this simple; the selection of 99% encircled energy apertures was based on a field with well isolated stars. Given our field and a seeing of 3.5″, we would never use an aperture as large as 10″ radius for the intensity extractions. Dropping the aperture size a little would give much improved results. Also in the case where much of the PSF width is due to an imposed defocus, then the 99% encircled energy radius of prime importance for predicting contamination grows more slowly. With a defocus of 2″ plus 1.5″ real seeing, the FWHM would approach 3.5″, but the PSF wings would drop much more quickly than for a pure 3.5″ seeing case, yielding a 99% encircled energy radius of only some 6″. In this case contamination should not be a problem as the seeing fluctuates by 0.3″. After considerable experimentation the defocus error term (units of ppm) was chosen as

$$\text{defocus penalty} = 1380 \exp[(\text{FWHM of PSF} - 1/\text{seeing} - 3.2)/0.3] X^{1.5}, \quad (6)$$

where the FWHM of PSF is the sum of seeing and defocus (defocus would be diameter of pupil image disk in perfect seeing) and X is the airmass. The airmass term is included as a rough means of allowing for larger and more variable seeing expected to correlate with large zenith distance.

With a time dependent error budget fully specified, the FORTRAN optimization code generated a simulated sequence of observations (in increasing hour angle) over a grid of defocus settings. Integration times were selected to set the central intensity of the brightest star to 75% of linearity range. The time series simulations were terminated when the rough sensitivity estimate

$$\text{sens} = 2\sigma(4/N_{\text{obs}})^{1/2} \quad (7)$$

reached a minimum, where σ is the time series rms and N_{obs} are the number of observations. Defined in this way sens corresponds to the height of 4σ peaks in a power spectrum of white noise. Figure 4 illustrates how this process was used to select optimal defocus settings for Kitt Peak and CFHT (excellent seeing) conditions. With excel-

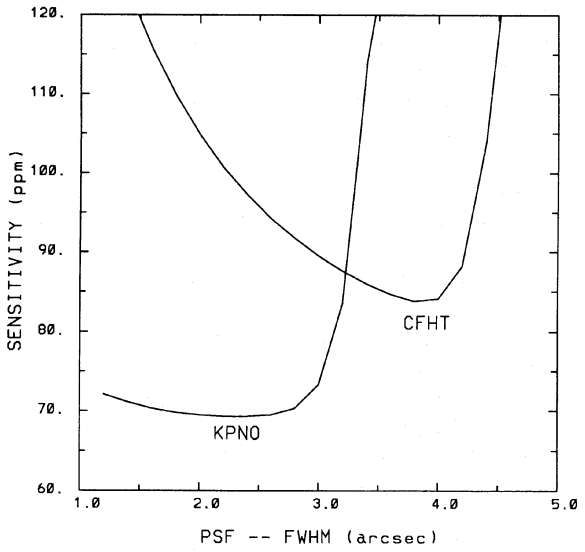

FIG. 4. Simulated nightly sensitivities in ppm for KPNO 4 m and CFHT 3.6 m telescopes vs point spread function FWHM. For KPNO and CFHT the assumed atmospheric seeing contributions were 1.2″ and 0.6″, respectively. Optimal defocus (plus seeing) settings were 2.2″, (KPNO) and 3.8″ (CFHT). The nightly sensitivities actually obtained at CFHT was nearly equal to the predicted KPNO level.

lent seeing at CFHT and little defocus the integration times are very short, resulting in most of the total time being spent cycling the CCD with resultant large noise level. Integration times corresponding to optimal defocus settings were 89 and 22 s for KPNO and CFHT, respectively. The nightly sensitivity at Kitt Peak was a very weak function of seeing plus defocus over a broad range. At CFHT and other sites with less favorable CCD well depth and image scale the dependence on PSF scale was much more pronounced.

One consideration in the selection of field and observing month was that M67 would not reach 5 h east until 3 h after sunset, but would reach 5 h west just at dawn. Therefore some time was available in the evening for empirically checking the setup optimization and practicing the data acquisition procedures. These may seem minor points of detail, but in reality such considerations contributed significantly to the project's reaching good precision at all sites. To facilitate the setup optimization an observing guide (from R.L.G. and T.M.B.) was distributed to all groups. The observing guide outlined in great detail how the observations and attendant calibrations should be done. A setup field in NGC 752 (7 h ahead of M67) was provided and test observations on it outlined to allow correcting in real time any uncertainties about the planning process. Specifically the NGC 752 field, consisting of three well isolated 10th–12th magnitude stars in a 60″ FOV, was used to refine estimates of the total system quantum efficiency, to correct as necessary the fraction of light hitting the central PSF pixel (used to fix integration time), and to check the degree of contamination 11″ away as a function of defocus.

Also given in the observing guide was an outline of calibrations to be acquired at each site (some nonstandard; this will be discussed in Sec. 4), and an admonishment to verify the header times and to supply an algorithm that explicitly alowed estimation of time (UT) at midexposure. Advice was also given to carefully monitor guiding and to correct for drifts when necessary with autoguiding systems.

Given that we wished to observe with the brightest star only 25%–40% below saturation to maintain a good combination of focus and high duty cycle, sites were often "pushing the envelope" of allowed focus and integration time. Less than 1% of potential observing time was compromised due to breakdown of observing procedures.

TABLE 2. Time series summaries.

Site	N_{obs}	Hours	Duty cycle	rms-16	sens-16
KPNO	1251	33.5	0.75	326	36.9
HALE	1389	50.3	0.59	320	34.3
CFHT	1747	25.5	0.67	390	37.3
AAT	880	20.8	0.71	440	59.3
CAA	354	6.2	0.44	510	108.4
NOT	1903	20.3	0.65	923	84.6
sum	7524	156.6			

3. OBSERVATIONS

The primary goal for all sites was to obtain time series observations for as long as possible each night on the M67 field shown in Fig. 1. The M67 time series were all acquired using the same Corning 4-96 filter (except at the NOT as noted). Most sites also acquired short time series on the brighter NGC 752 setup field; these sequences were useful for defining details of the error budget and will be discussed in Sec. *4.7*. Here we provide an overview of the M67 time series in Table 2, then discuss details of each site starting with Kitt Peak and moving westward. Here Duty cycle is defined as exposure time divided by the sum of exposure time and readout time for the CCDs in use at the given site. Columns rms and sens refer to star No. 16 of the ensemble. The sensitivity is as defined in Eq. (7). Note that although some of the contributing telescopes had apertures of less than 4 m, the time averaged aperture size from Table 2 is marginally in excess of 4 m.

Overall the observations provided a time base of 5.98 days with a duty cycle (at least one site acquiring M67 time series) of 64%. For 30% of the time more than one site was active and for short periods four telescopes were observing simultaneously. This is an excellent duty cycle, but the true significance will only become clear in Secs. 5 and 6 when we discuss details of the total data set relative to the goal of detecting oscillations.

The total data set from all sites, including time series on M67, NGC 752 and calibration frames, consisted of over 17 000 CCD images or about 11 GB. Data from all sites was sent to ST ScI on Exabyte tapes with reductions and analyses performed on SPARC2 class computers.

TABLE 3. M67 time series, KPNO 4 m.

Date	Jan 13	Jan 14	Jan 15	Jan 16	Jan 17	Total
No.	229	302	299	42	380	1252
T_{exp}	75.0	81.2	70.5	80.0	63.8	72.2
Hours	6.4	9.1	8.0	1.2	8.8	33.5
Star	time series rms in parts per million					
12	258	266	334	532	347	317
13	314	294	393	473	480	389
16	268	266	339	462	372	326
27	358	301	413	364	447	387
28	501	361	448	544	455	443
37	448	361	489	399	666	513
41	378	332	517	393	492	441
44	393	323	489	794	701	528
48	387	355	450	497	475	425
49	392	356	458	557	470	427
52	407	336	468	547	529	450
65	595	512	711	536	709	639

TABLE 4. M67 time series, Palomar 5 m.

Date	Jan 12	Jan 13	Jan 14	Jan 15	Jan 16	Jan 17	Jan 18	Total
No.	40	229	255	213	162	257	233	1389
T_{exp}	90.0	69.4	63.8	90.0	85.2	62.7	60	71.2
Hours	1.7	8.1	8.5	8.7	7.4	8.7	7.2	50.3
Star	time series rms in parts per million							
12	408	363	259	362	321	332	314	327
13	512	319	300	333	424	366	358	350
16	433	313	291	351	298	369	288	320
27	370	271	309	357	365	329	379	333
28	429	339	322	303	346	369	333	336
37	481	333	302	373	330	377	403	356
41	735	383	357	396	358	487	420	414
44	629	466	430	538	445	461	439	465
48	802	441	413	422	580	451	404	457
49	862	469	401	447	654	414	470	475
52	513	462	389	504	484	515	470	469
65	1480	739	722	1072	890	726	740	836

3.1 Kitt Peak National Observatory

The 4 m telescope at KPNO was used from 1992 January 12–17 (R. L. G. and L. P.) with the TEK 512×512 (T5HA) AR-coated CCD mounted at the seldom used (for CCD imaging) RC focus. At the $f/8$ focus the 27μ pixel scale was 0.18″ providing a 92″ FOV. Observing conditions varied from poor (very high winds and $\geqslant$4″ seeing on the 16th) to good (clear and generally stable 1.5″ seeing) on the 14th, although even on the best night conditions probably were not "photometric." A CCD gain of 17.6e^-/ADU was used throughout. Exposure times varied from 60–95 s depending on conditions. With the new observing control protocol, ICE, available under IRAF, we generally initiated an observing script at the beginning of each nightly sequence with a smoothly varying integration time expected to cancel out the changing extinction with airmass. CCD readout overhead was 24.5 s for the first four nights and 18.6 s for the final two. The control system was using a valuable (to us!) 6 s to establish a handshake with the telescope control computer in order to load target coordinates into the header. We had this feature turned off for the final two nights. A minor zero point shift in header UT times was noted (and corrected for in the analyses.) As reflected in Table 3 the general observing conditions changed significantly through the week. The 12th of January was marked by high winds, heavy snow and lightning. Conditions were still in transition on the 13th (initially quite poor seeing with significant variability throughout). January 14 was the best night, but by the 15th winds were picking up and on the 16th most of the night was lost due to wind speed above the limit for opening the dome. Wind speeds were also high on January 17, but allowed observing. Table 3 gives nightly summaries. The line labeled No. gives number of images in the primary M67 time series. T_{exp} is the mean integration time in seconds. Hours is the full extent of primary time series.

Further discussion of the error budget will appear in Sec. *4.7*. The rms entries for Table 3 include all of the calibrations, reductions and time series processing steps as discussed in Sec. 4, but do not allow for time variable weights. In Table 3 and the others to come in Secs. *3.2–3.7* results are only from the reductions performed by R. L. G.; as discussed in Sec. *4.8* a minor gain is accomplished by performing a weighted average with the independent results from H. K.

3.2 Palomar 5 m

The 5 m telescope at Palomar (J.K.M. and M.L.P.) was used 1992 January 12–18 with an AR-coated TEK 1024 ×1024 CCD. In support of the M67 oscillations project a CCD mounting base instrument (shutter, filter, offset guider, etc.) was developed by McCarthy (1992). The need for a new CCD camera was driven by the poor match of the existing focal positions ($f/16$ Cass or $f/3.4$ prime focus) to the project needs. The Cassegrain focus allowed only a 63″ FOV, which would have covered only half of the desired ensemble; the prime focus gave a pixel scale of 0.3″, which would have given unacceptably high single-pixel count rates. Also there was no provision at prime focus for a TEK CCD, so utilization of prime focus would also have required development effort. An $f/9$ focal reducer was available for the 5 m Cassegrain focus and provided an ideal pixel scale of 0.11″ and 110″ FOV for this project. A CCD gain of 11.3e^-/ADU was adopted and exposure levels were kept below $1.5\times10^5e^-$/pixel to assure linearity. Integration times were 60–90 s with a 50 s readout time overhead. Given the favorable pixel scale, slight defocus was required on only one occasion (January 14), when the seeing approached 1 arcsec. In general the observing conditions at Palomar tracked those at Kitt Peak in terms of wind conditions and seeing. About 1 h of data was rejected for each of January 16 and 18 when seeing and/or transparency degraded beyond acceptable conditions. Table 4 details the nightly time series quality for each star.

As reflected by the entries in Table 2, the Palomar sensitivities were about 10% better than from any other site for the best stars and, thanks to lower relative noise on fainter stars, averaged about 20% better. This superior per-

TABLE 5. M67 time series, CFHT 3.6 m.

Date	Jan 13	Jan 14	Jan 17	Total
No.	601	497	649	1747
T_{exp}	31.6	36.2	31.4	32.8
Hours	8.6	7.9	9.0	25.5
Star		rms in parts per million		
12	375	353	416	386
13	375	365	454	404
16	396	353	410	359
27	475	436	495	470
28	508	507	589	538
37	539	458	594	538
41	490	476	611	533
44	597	533	705	622
48	574	590	667	612
49	598	672	719	665
52	634	611	681	611
65	897	821	1053	935

formance was also associated with the greatest supporting efforts in all stages of the project. The Palomar application deadline in October for January observing left very little time for a significant instrument development effort (McCarthy 1992). The large format CCD being read out at a rapid cadence, coupled with the many lengthy calibration sequences (Sec. 4) and seven clear nights in a row taxed the data acquisition system and two observers to their limits. The resulting data set from Palomar generated fully half the total campaign storage requirement and coupled with a more difficult than usual reduction process (see Sec. *4.3*), required about half the total effort for the reductions.

3.3 Canada–France–Hawaii 3.6 m

The 3.6 m CFHT was used (P.B.S. and T.M.B.) 1992 January 13–17 with the RCA4 CCD. We had requested the $f/8$ Cassegrain mount, but were obliged to use the $f/4$ prime focus, giving a pixel scale of 0.2″ for the 15μ pixels. A region of 470×470 (from full 640×1024) was read out, providing a 95″ FOV. The readout and CCD overhead cycling time was 18.7 s. RCA4 is claimed to be linear to $6\times10^4 e^-$ per pixel. As already discussed in Sec. *2.3* the excellent CFHT seeing, coupled with a rather shallow well-depth CCD mounted at prime focus, created severe planning constraints. Nonetheless a careful balancing of telescope defocus and integration time was maintained. CFHT provided the best precision per unit time of any site. The conditions on all three observing nights were considered to be photometric in quality. On the night of January 13 the seeing was subarcsec; a defocus of up to 4″ was applied to maintain adequate image spread. Seeing was closer to 1 arcsec and slightly variable on the 14th leading to a more variable PSF, but the conditions were still excellent. The nights of January 15 and 16 were lost to blizzard conditions on Mauna Kea. On the 17th there was a short period of seeing variable to 3.5″, but most of the night was characterized by a PSF stable at about 2 arcsec. Table 5 details the time series properties from CFHT.

TABLE 6. M67 time series, AAT 3.9 m.

Date	Jan 14	Jan 15	Jan 16	Jan 17	Total
No.	152	266	177	285	880
Hours	3.6	6.3	4.2	6.7	20.8
Star		rms in parts per million			
12	469	563	722	513	565
13	436	448	621	555	515
16	336	348	499	521	440
27	480	491	639	583	548
28	472	459	606	629	549
37	429	541	642	648	580
41	479	503	697	663	593
44	514	584	676	658	615
48	443	510	657	666	580
49	476	481	644	673	578

3.4 Anglo-Australian Telescope 3.9 m

The 3.9 m AAT was used (L.E.C. and J.P.) 1992 January 14–17 with an RCA CCD. The $f/8$ Cassegrain mount provided an image scale of 0.20″ per 30μ pixel and an FOV of 61×102 arcsec with this 320×512 pixel CCD. This was smaller in one dimension than the nominal FOV, but with proper rotation all stars with the exception of Nos. 52 and 65 from the primary ensemble were covered (No. 12 was sometimes close to an edge, contributing to higher than nominal noise). On January 14 2 h of data were dropped at the beginning and about 1 h from the time series end when seeing exceeded 4″. The seeing on January 15 was excellent, reaching a maximum of 2.5″ at the end of the night; seeing of about 1″ was encountered 2 h into the time series leading to saturation of star No. 12 on a handful of frames and requiring a defocus to be introduced. Two hours at the end of the 16th were excluded due to seeing in excess of 4″ coupled with variable extinction and a bright sky. The 17th was marked by generally stable conditions with seeing of 2″–2.5″. Table 6 provides details of the night by night results at the AAT. Observations at the AAT were made close to the austral solstice, and hence the observing periods were shorter than at the northern sites. Additionally, the setup field NGC 752 was not accessible.

3.5 Kavalur 2.3 m

The 2.3 m at Kavalur was assigned for the nights 1992 January 12–15 (M. P.). Unfortunately this site did not acquire any data on M67 due to poor weather. On balance the network as a whole fared well with the weather conditions.

3.6 Calar Alto 3.6 m

The 3.6 m telescope at Calar Alto in Spain was used for the nights 1992 January 15–17 (H.S. and W.W.W.) with an RCA 640×1024 CCD with 15μ pixels. The image scale of 0.25 arcsec per pixel provided a large field of view as all pixels were read out, but only data for the 100″ field of interest were analyzed. An integration time of 28 s was used with a readout overhead of 26 s. Only the final night

TABLE 7. M67 time series, CAA 3.6 m.

Star	amp
12	492
13	567
16	510
27	649
28	603
37	694
41	671
44	778
48	734
49	781
52	712
65	1186

(January 17) was clear and high humidity forced the dome to be closed for 2 h at midnight. Despite the relatively small amount of data provided, the unique longitude and time allowed an important contribution to the overall network. The time series precisions from Calar Alto are shown in Table 7. The total time series spanned 8.5 h with a 2.3 h gap for a total of 354 integrations. Seeing (plus defocus) was fairly stable at about 2″–2.5″ with no frames in excess of 3.5″.

3.7 Nordic Optical Telescope 2.5 m

The 2.5 m NOT was used for the nights January 13–17 (S.F., H.K., J.A.B., and I.V.) with a TEK 512×512 CCD. The CCD was used in the imaging mode of a low-dispersion spectrograph/imaging instrument. The image scale of 0.5″ per 30μ pixel supplied a 95″ FOV with a readout of 190×190 pixels. The CCD was operated at a gain of 13.5e^-/ADU and had a readout overhead time of 9.0 s. All integrations were 25 s for the M67 time series. Weather conditions were fair for the nights of January 13 and 14 with a few short periods at the beginning of both nights experiencing light cirrus (extinction limited to 10%–25%). The CCD ensemble photometry could cope with these minor cirrus problems without significantly increased noise levels. On January 15 the effect of cirrus was much more pronounced with a mean extinction of 30% to 40% with fluctuations of up to a factor of two for the best 3 h period. Data were obtained on the remainder of January 15 and parts of January 16 and 17, but were of much lower quality than that for the first two nights. Seeing plus defocus varied over 2″–3.5″ each night. Table 8 details the high quality results from the NOT. The use of a beam splitter created ghost images at a 1% relative intensity level offset by 17″ to the East. This led to near coincidences of real images and ghosts in four cases. The worst case was a relative intensity ghost of 0.4%, 3.1″ away from star No. 16 generated by star No. 48. Although a rather minor effect, at our extreme precisions this ghosting may explain the relatively larger error seen in star No. 16 as compared to star No. 12 (compare with KPNO results). The larger rms from NOT follows from using the shortest integration times and the smaller aperture. The large number of data points compensates, and these data provide a valuable overall contribution.

TABLE 8. M67 time series, NOT 2.5 m.

Date	Jan 13	Jan 14	Jan 15	Total
No.	798	853	252	1903
Hours	8.4	8.9	3.0	20.3
Star		rms in parts per million		
12	774	601	715	700
13	852	741	898	809
16	911	924	1020	923
27	1039	884	1034	969
28	960	926	1066	957
37	968	919	1129	966
41	1091	973	1023	1025
44	1093	1088	1527	1154
48	1146	1042	1210	1104
49	1160	1042	1263	1120
52	1204	1106	1368	1181
65	1626	1529	1933	1622

4. CALIBRATIONS AND DATA REDUCTIONS

4.1 Basic CCD Calibrations

Since we were attempting more precise measurements with CCDs than are commonly attempted, usually with specific CCDs that had never been used in this way, an extensive suite of calibration observations was requested from each site. Most of the calibrations were routine: numerous biases, darks, dome and twilight flats at all sites. Analysis of these calibrations showed no significant problems at any site. Corrections were applied in routine ways for: (1) overscan subtraction, (2) bias subtraction (not needed at most sites), (3) dark subtraction, and (4) flat-field normalization. Any nonlinearity corrections as discussed below were applied before the flatfielding operation. A final step in the reduction of all frames was subtraction of a mean sky intensity. Several options for evaluation of sky were tried: simple mean of the clear region, histogram generation and Gaussian centroiding, and fitting of a plane to clear regions. Sky subtraction was not a critical issue for this program and different approaches showed little difference in resulting noise level for the primary ensemble stars. All CCD reductions, including the linearity analyses to be discussed next, were performed by R.L.G. unless otherwise specified.

Linearity, or rather the possible lack thereof, was a particular concern. Although CCDs are widely and justifiably touted for their linearity properties, some devices deviate from a perfect linear response at high or low light levels. To a large extent a well executed program of CCD ensemble photometry is immune to minor CCD defects. As an example: in principle flatfielding is not important—we care only about relative changes of an individual star's intensity over time; if guiding and seeing are steady the flatfield problems will not influence the differential time series. But of course guiding and seeing are not perfect and even for fully differential, relative photometry it is necessary to have decent flat fields if additional error terms are to be kept under 100 μmags. Likewise for deviations from linearity,

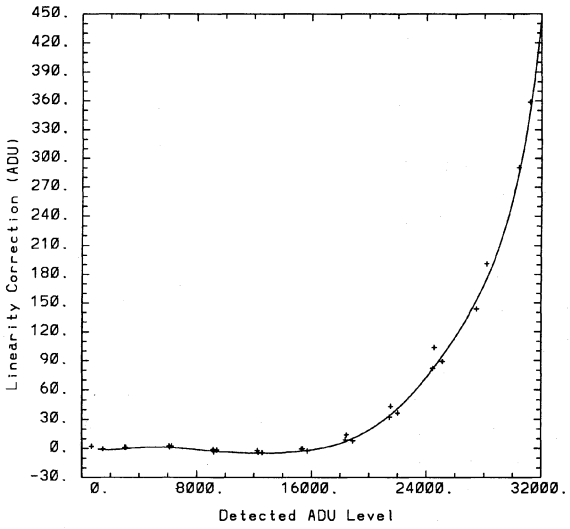

FIG. 5. High intensity linearity calibration for the KPNO T5HA CCD. CCD saturation occurs at about $5.5\times10^5e^-$ or 3.2×10^4 ADU at the gain in use. The ordinate gives the correction to be added to a given input level to restore linearity. A 1% deviation from perfect linearity occurs at $\sim3\times10^4$ ADU per pixel. Solid curve is a high order polynomial fit. Characterization was stable to about 0.1% in independent trials.

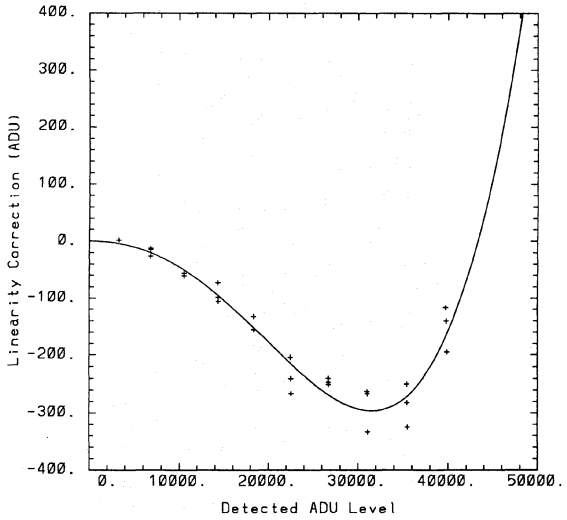

FIG. 6. Correction term to quadratic nonlinearity term for the AAT RCA CCD. Quadratic term [Eq. (8) with $\alpha=5.6\times10^{-7}$] amounts to 20% deviation at $3\times10^5e^-$. These deviations amount to $\sim\pm1$% and are represented by a fourth-order polynomial. The extrapolation past 40 000 ADU cannot be considered significant, but this affects a negligible fraction of the data.

the ensemble normalization process removes problems to first order, but with fluctuations of seeing and extinction different portions of PSFs sample separate deviations from linearity and do not cancel perfectly. One CCD, the RCA used at the AAT, had a builtin nonlinearity on the order of 20% at high intensity (Robinson *et al.* 1989) that was routinely compensated for in data reductions. To better characterize the AAT device and to guard against smaller nonlinearities possibly existing at other sites, we devised programs for explicit nonlinearity test calibration. The high and low intensity versions are discussed in the next subsections.

4.2 Nonlinearity at High Intensity

Most CCDs have stipulated linearity ranges based upon laboratory characterization with stable light sources. Because of the need to count extremely large numbers of photons per CCD readout our observations often entered domains where nonlinearity could become an issue. It seems to be common, albeit incorrect, knowledge that a good characterization of CCD linearity cannot be accomplished at the telescope, since flatfield lamps are unlikely to be constant to the requisite level of order 10^{-3}. However, if the calibration lamps do not drift, or flicker, on a rapid time scale (most seem not to in practice), then a calibration experiment with a control integration interleaved to monitor slow changes in lamp brightness should be capable of deriving an excellent linearity curve. To be specific: assume lamp intensities for flat fields are adjusted such that a 3 s integration yields an exposure to 10% of saturation, then sequences of 3 s, 6 s,... 3 s, 6 s; 3 s, 9 s,... 3 s, 9 s;...; 3 s, 27 s,... 3 s, 27 s will map out linearity at 20%, 30%,... 90% of full well depth. Most sites performed experiments of this type, with good calibrations of nonlinearity resulting.

Figure 5 shows the nonlinearity characterization for the CCD used at Kitt Peak. The central exposure was 6 s yielding about 10% of saturation. Nearly all M67 exposures at Kitt Peak were acquired with peak intensity levels less than 75% of saturation where the nonlinearity is only 0.3%. The nonlinearity leads to time series errors as a second order effect, i.e., following seeing fluctuations that change the relative contribution of total light to different parts of the nonlinear domain on a frame to frame and star-by-star basis. Some fraction of induced nonlinearity errors will also be removed in the ensemble normalization and time series decorrelation steps. Application of the small nonlinearity correction shown in Fig. 5 to the reduction of KPNO data had no discernible effect on time series quality. Similar results using this approach were found for the Palomar, Calar Alto, and NOT data: high intensity nonlinearity was verified to be small and did not require data calibration. At CFHT a different approach (Stetson 1989) using graded exposure times on a rich field of stars with a range of brightness was used to verify good linearity. To further check that a linearity problem was not introducing noise most sites acquired short sequences on the NGC 752 setup field in which different exposure times were alternated. Subsequent reductions showed no appreciable "signal" of the forced exposure level changes after normalization to the ensemble mean (an exception to this will be discussed in Sec. *4.3*).

The AAT was the only site where high intensity nonlinearity was important. By design, to improve other qualities, the RCA CCD at the AAT had a nonlinearity of

$$N(\text{measured in ADU}) = N[(\text{actual})(1+\alpha N(\text{actual})], \quad (8)$$

where $\alpha = 6.67\times10^{-7}\times\text{gain}$ (gain $= 9.4e^-$/ADU). This results in a 20% correction at $3\times10^5 e^-$ per pixel and was thought to be accurate to about 3%. We performed a high intensity nonlinearity experiment at the telescope as described above and tried fitting the quadratic equation to the results. A value of $\alpha = 5.6\times10^{-7}$ gave a best fit (assumed gain = 9.4), but coherent deviations of $\sim$1% were still present as shown in Fig. 6. The full nonlinearity could be represented by a fourth-order polynomial with residuals at the level of 0.2%, consistent with limits set by the measurements. Correcting for the CCD nonlinearity was quite important as verified by trial analyses with and without inclusion of this reduction step. Although the ensemble normalization and time series decorrelation steps can remove much of the impact, with no explicit treatment of the nonlinearity in the reduction step the final results would be worse by about 20% for the average star and 60% for the worst cases (in terms of time series rms). The high intensity nonlinearity experiment executed during the run enabled a good calibration of the nonlinearity. Final results would be worse by a few percent on average to 40% on the most sensitive stars using the prerun linearity equation only. The smooth error distribution with stellar magnitude shown in Table 6, and generally low noise level suggests that ultimately the CCD nonlinearity was not a problem for this demanding observation.

4.3 Nonlinearity at Low Intensity

Most CCDs have at least isolated regions that respond nonlinearly to light at low intensity. This effect is a result of localized charge traps in the imaging region or in the shift register and is sometimes referred to as deferred charge, or charge skimming. A formula found to work well in compensating for charge skimming (Stetson 1991) is

$$\text{true}-\text{observed} = \text{skim}\times[1-\exp(-0.56\times\text{true}/\text{skim})], \quad (9)$$

where "skim" is the asymptote—the number of electrons (or ADU) that are skimmed from a pixel originally containing many electrons. In order to detect and if possible calibrate out deferred charge problems each site acquired a large (50 to 100 at each level) number of low intensity flat fields at mean levels of 200, 400, and 800 e^- by successively doubling the exposure time. These could then be averaged together and used to solve for a deferred charge map (Gilliland & Brown 1988). For most sites this detected a few bad columns or charge traps (CCDs available to these telescopes were in general high quality devices). Correction for these minor defects was not an important reduction step for this project, as some effort was made during setup to locate the ensemble stars away from known defects.

These calibration sets did, however, yield information on general linearity of the readout amplifier at low light levels. From the Kitt Peak calibrations the mean intensity of five different exposure levels from $\sim$185 to 2885 e^- in

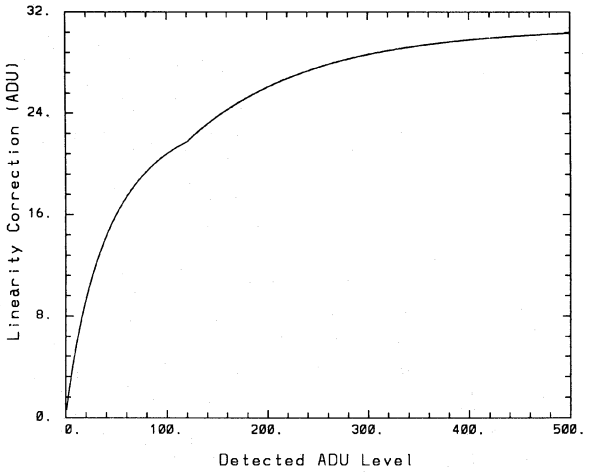

FIG. 7. Low intensity linearity calibration curve for the Palomar CCD. The ordinate gives the correction to be added to a given input level to restore linearity.

factor of two steps fell within a $\pm$1% range of linear about the central intensity. Unfortunately these sequences were not taken with interleaved control exposures so we do not know if the lamp drifted by 1% on an hour time scale, or if this was indicative of a real CCD nonlinearity. In any case this small deviation from linearity would not be a problem for the ensemble photometry.

The low intensity calibration sequences obtained at Palomar showed a full range deviation of 35% from linearity. Four sequences of exposures at successive factor of two levels in integration time gave means of 6.27, 14.6, 31.4, and 67.8 ADU, respectively. Each successive step shows more than a doubling of intensity. Again, the sequences were not obtained with interleaved control exposures (a minor breakdown in our preplanning advice) so a variation of lamp intensity could have been the cause of the apparent nonlinearity. This calibration set was analyzed for localized deferred charge problems; when none of consequence were found, the set was put aside. The Palomar data set was by chance the last to be reduced. Reductions of calibrations and time series from all other sites had gone smoothly—basic CCD calibrations were worked through, reductions done, intensity extractions performed, and differential time series were then produced. The first production of time series for a given site was usually rewarded with well behaved results, or if not, an obvious explanation existed like the seeing approaching or exceeding 4″ for parts of the data set. The first Palomar time series produced had errors fully twice as high as expected. Inspection of the Tables in Sec. *3.1–3.7* show a smooth increase of rms from bright to faint stars. The initial Palomar results had the largest errors symmetric about stars of average brightness—consistent with a linearity problem. (The high intensity nonlinearity data for Palomar had already been processed, showing deviations very similar to those in Fig. 5 for Kitt Peak, i.e., a very linear chip.) Further work showed that the time series developed problems during the

transition period from bright to dark sky at moonset; again suggestive of a nonlinearity, but in this case well correlated with sky brightness! After a great deal of analysis, it was found that application of the low-intensity nonlinearity correction shown in Fig. 7 during the CCD reduction stage restored a well behaved distribution of time series rms noise versus stellar brightness. The general form of the curve in Fig. 7 follows Eq. (9), but with two different exponential scale terms at different intensity levels merged together. The nonlinearity correction was derived by trial and error guided by an in-depth monitoring of which nonlinearity term added during the ensemble normalization process would yield best results. (The low intensity nonlinearity could be accommodated in the ensemble normalization stage by including a constant term in addition to the usual multiplicative factor. At times of high sky background the full range of ensemble star intensities would normalize with the constant term near zero; with dark sky the constant term was large and positive to maintain linearity with conditions holding with a bright sky. This two-term ensemble normalization worked too well, in that the rms for the brightest stars was reduced below Poisson and scintillation limits. As a diagnostic of residual nonlinearity, plotting the constant term versus sky brightness was powerful, but final analysis required application of the nonlinearity correction in the CCD reduction stage and time series normalization with just the standard single term.) The correction is also generally consistent with the low-intensity calibration sequence means noted earlier. A more robust low-intensity calibration experiment with interleaved control exposures would have yielded the appropriate correction straight away. Test sequences on NGC 752 acquired with alternating exposure times differing by 20% showed a full order of magnitude reduction of power at the Nyquist frequency with inclusion of the nonlinearity correction.

As with the AAT CCD nonlinearity, we believe the correction for the Palomar CCD to be sufficiently precise that little residual noise can be attributed to it. With the proper nonlinearity correction the Palomar data set yields the best overall single-site sensitivity, without this correction the sensitivity would not have met that obtained in half the observation time by the smaller AAT.

4.4 Intensity Extractions

In the remainder of Sec. 4 and all of Secs. 5 and 6, fully independent analyses have been done by R. L. G. and H. K. with some independent analyses by others. It is our goal to quantify what oscillatory signals may be present in the rich data set described above; we have therefore tried to maintain independent analyses in the hopes of identifying any shortcomings in different approaches. Where appropriate at intermediate stages we have compared and combined results before proceeding to the next analysis stage.

Turning a time series of reduced two-dimensional images (now cleared of any flat field, dark, linearity, etc., defects) into a time series of stellar image intensities is the central problem of CCD ensemble photometry. Our problem shares many aspects with "classical" CCD photometry reduction packages such as the widely used DAOPHOT (Stetson 1987), but there are subtle differences of approach. Available CCD photometry packages are usually geared toward the most rapid and efficient possible measurement of stellar intensities consistent with desired precision $\sim 1\%$ or better. Much of the machinery in standard packages has been developed to handle crowded star fields. Our problem is different: in principle we care not a whit about absolute photometry, but we care a great deal about maintaining precisely the same relative intensity extractions across different frames in the time series. Nature makes our problem difficult through seeing variations over time that change image characteristics; by keeping the analysis strictly consistent from frame to frame we avoid exacerbating this problem. By design we are not dealing with crowded fields; once our ensemble stars start overlapping to the extent that multiple star PSF fitting is required, the resulting errors would be far larger than acceptable.

We have used two separate packages for the intensity extractions; descriptions may be found in: KF92, Gilliland & Brown 1988, and G91. Differences between our independent approaches will be noted only if they seem important for a general discussion. But a few words are in order about intensity extractions for the ensemble of stars shown in Fig. 1. For extremely high precision work on isolated stars digital aperture photometry is likely to work as well, if not better than PSF fitting in most cases. In applying aperture photometry the reduction program needs to know: (1) what size aperture to use, and (2) where to center the aperture for each star. The optimal aperture size is different for separate stars given their unique crowding characteristics. As an example consider stars No. 37 and 49, the first of which is very well isolated, while the latter has multiple, brighter neighbors only 12″ away. A large aperture would work well for No. 37, while a smaller aperture would be best for No. 49 to minimize contamination from neighbors. Can we simply do intensity extractions in which each star is assigned its intrinsically best aperture? No, as that would violate the most fundamental constraint of CCD ensemble photometry, namely that all stars in the ensemble must be processed identically within a given frame and (as nearly as possible) identically across frames. The reason for this is simple: as seeing fluctuates, different fractions of the total intensity fall into different aperture sizes; if two stars are assigned apertures of different size their response to a seeing change will be inconsistent and ensemble normalization will not cancel the atmospherically induced changes. If both stars are extracted with identical apertures, then no matter what seeing or guiding does to PSFs in a given exposure, they both experience the same relative response and normalization to the ensemble mean works well. But to give an explicit example of how different stars would benefit from use of unique apertures consider the following. A reduction of the Palomar data set for January 15 with a digital aperture size of 8000 pixels (radius of 5.4″) yields time series rms of 373 and 844 ppm for stars No. 37 and 49, respectively. A similar ensemble normalization reduction sequence using an aperture size of

2285 pixels (radius of 2.9″) yields noise levels of 549 and 447 ppm for Nos. 37 and 49, respectively. As expected, optimal aperture sizes are inversely correlated with local crowding. The optimal aperture size differs from star to star from signal-to-noise considerations as well (Howell 1989; Stetson 1990). We cannot run a single intensity extraction sequence in which star No. 37 is assigned 8000 pixels and No. 49 is assigned only 2285 pixels. We could adopt a compromise solution using an aperture size that optimizes results for the twelve ensemble stars on average. But a better approach is to run complete and fully independent intensity extraction and ensemble normalization sequences in which all aperture sizes are identical within each sequence, but vary from sequence to sequence. Then we can choose to use the time series for star No. 37 from one case and the time series for star No. 49 from another. In this way optimal aperture sizes can be used for each star.

Other stars, e.g., No. 138 (not a member of the normalization ensemble, but followed for reasons of serendipity) yields best photometry if processed with a PSF fitting in which the much brighter neighbor is fit simultaneously. Therefore, in practice we have performed for all nightly data sets a large set of autonomous intensity extractions with internally consistent treatment of normalization, and we then selected the best case for each star from this set. Most stars yield optimal results over a fairly narrow range of intensity extraction parameters; the above extreme examples were chosen for emphasis. In previous observing programs we had tried different control parameters, but had always selected the single approach (aperture, or PSF radius) that gave best average results for the full ensemble. This new approach is based on sound recognition that different control parameters will work best for separate stars and allows more nearly optimal results for all of the stars.

Beyond a few tedious coding changes to account for much larger images (in pixel number) in this project than previously encountered, no real changes to the existing intensity extraction packages were required. Given the added complication of very defocused images from some sites it was a pleasant surprise that the existing PSF fitting approaches (GB88, and KF92—the latter package called MOMF had been developed partially with defocused images in mind) performed well. There are significant differences between the approaches of KF92 and GB88. The latter assumes sky has been removed globally as a reduction process and fits PSFs without a background term, while the former allows local sky as a free parameter in the PSF fits (i.e., it does not matter if a global term has been subtracted already). One of us (R.L.G.) thought the global subtraction with assumption of zero background for PSF fitting should be superior for this project, but testing by H.K. showed that MOMF extractions really did benefit from allowing local sky to vary. KF92 describe a PSF extraction that includes addition of "residual aperture photometry" obtained by adding back in the aperture sum evaluated after subtraction of the PSF fit to a stellar image. One of us (H.K.) thought the PSF plus residuals approach should be superior for this program, but testing by R.L.G. showed that doing so compromised the results of his analyses. Both packages yield generally consistent and excellent results; we did not find improvements by attempting to include each other's "essential" steps. In treatment of such a complex problem there is not a well constrained set of approaches that will work best. We have found that our full, independent approaches reach similar precision levels, but that application of particular steps useful for one of us does not necessarily result in better results if included piecemeal in the other's analysis.

4.5 Ensemble Normalizations

The basis behind CCD ensemble normalization is simple. We assume that fluctuations frame-to-frame induced by changes in atmospheric properties are coherent over the full frame. This is generally an excellent assumption even when highly nonphotometric conditions exist (e.g., see Figs. 1 and 2 of GB92 showing the remarkably similar raw intensity tracings for separate ensemble stars with gross extinction changes and the resulting time series after normalization to the ensemble mean). With a substantial ensemble of stars (10 or more) in a small FOV (a few arcminutes or less) CCD ensemble normalization is very effective in removing atmospheric transparency variations. For this project with twelve ensemble stars we have chosen only to apply normalization to the ensemble mean (usually taken as average intensity for each star over 10 frames near meridian passage). With more stars in the ensemble (see GB91) color and position terms may also be included. In the present case with only one very red star (No. 12), allowing a color term would effectively allow one degree of normalization freedom to this one star, resulting in a time series in which real fluctuations are artificially suppressed.

We allow separate weights on each of the ensemble normalization stars. The weights are set iteratively in the following convergent process which in general results in the lowest mean time series rms over all the stars. (1) Start with weights = 1.0 for each star and perform one round of ensemble normalization (plus time series processing as discussed in the next subsection). (2) Reset weights normalized to a mean of unity inversely proportional to the time series rms squared for each star. (3) Repeat a weighted ensemble normalization of the time series. (4) Iterate steps (2) and (3) until convergence.

With this procedure (used by R.L.G.) a star is a member of its own ensemble for normalization. This leads to a self-suppression of intrinsic noise and real signal (if there is one), in which the time series variance (rms^2) is incorrectly reduced in proportion to the star's fractional weight. We guard against a runaway of this iterative process by: (1) resetting the rms for each star to correct for this self-suppression, and (2) not allowing the weight of any individual star to exceed 2.0, or $\frac{1}{6}$ the total for our case. A star of maximum weight will have incorrectly suppressed its own noise (or signal) by only 9%. All time series precisions quoted in this paper have already been corrected for self-suppression by the appropriate factor.

The time series analyses conducted by H.K. were done

without a star being included as a member of its normalization ensemble. The ensemble normalization was performed in this case in the same way as described in the next section for decorrelations against fluctuations in external parameters.

4.6 Time Series Processing

Having performed intensity extractions for all the ensemble stars for each frame on a given night one has much auxiliary information available in addition to the raw intensity time series. From the PSF fitting comes a precise measure of seeing and a mean position of the field in (x,y) CCD coordinates. From the earlier reduction process a time series of mean sky brightness is also available. Can use be made of these auxiliary time series to further improve the ensemble normalized intensity series? In general the answer is certainly yes. The essential argument justifying attempts to decorrelate the intensity time series against external parameters like the x and y position of the stars on the CCD is that any correlated "signal" is most likely noise in the intensity time series *induced by* fluctuation of the external parameter. In the case of a fluctuating image position on the CCD correlated noise will be produced if there are any residual flatfield errors. Note, however, that decorrelation against external parameters is a risky proposition if not done with extreme caution, thought, and testing. If a given star has a real variation at low frequency, a low frequency signal almost always present in the external parameters will almost certainly remove it. In our case we are not interested in low frequency information in our stars and decorrelation is a safe and prudent thing to do. Gains of 20% in rms noise levels are common with larger gains occurring for stars particularly susceptible to noise correlated with, and induced by, the external parameters. For example star No. 49 will benefit more from decorrelation against seeing than will No. 37, which suffers much less from contamination by neighbors.

In order to better control noise in the time series for the frequencies of primary interest ($\geqslant$400 μHz$=1/2500$ s) we apply temporal filtering to remove variations slower than about 1 h. (R.L.G. performs a Gaussian convolution and subtracts the resulting time series of low frequency variations. H.K. performs a local linear fit and subtracts this. The two approaches provide similar suppression of low frequencies.) This is done before decorrelation and prevents irrelevant but large low frequency components from dominating the decorrelation. The filter yields power spectrum responses of about 90% at 350 μHz, 50% at 200 μHz, and 10% at 120 μHz. This filtering reduces the inherent $1/f$ noise such that the resulting power spectrum is nearly flat at all frequencies.

4.7 Analysis of Error Budget

We expect two irreducible terms to contribute noise to every stellar time series: Poisson statistics on the number of detected photons and atmospheric scintillation. A third term, the contribution of readout noise and Poisson statistics on the background, will always contribute, but can be controlled to some extent through choice of digital aperture size or PSF weighting. Other sources of noise will sometimes play a role: incorrect subtraction of the background sky level, intensity uncertainties induced by image overlap from too much seeing or defocus, uncompensated nonlinearities, etc. We will generally isolate the sources of noise into three terms that are relatively easy to characterize: Poisson statistics, atmospheric scintillation, sky background plus readout noise, and a fourth all-encompassing term of everything else, also referred to as "reduction" noise.

TABLE 9. Atmospheric scintillation estimates.

Site	Date	T_{int}s	N_{obs}	Max counts e^-	scint
KPNO	Jan 14	10	180	3.8×10^7	125
KPNO	Jan 15	35	108	1.4×10^8	151
KPNO	Jan 17	21[1]	152	6.9×10^7	209
CFHT	Jan 14	40	60	1.1×10^8	126

[1]This was actually a sequence with times of 16, 20, 22.4 and 28 s interleaved to test for nonlinearity residuals.

Poisson noise on the object is trivially known as the square root of the total number of detected photons. Likewise the contributions of readout noise and sky background (at least for aperture photometry) are easily estimated as

$$(\text{readout}+\text{sky})=[n_{\text{px}}(s+\text{ro}^2)]^{1/2}, \quad (10)$$

where n_{px} is the number of pixels in the aperture, s is the sky level per pixel, and ro is the CCD readout noise. To our knowledge atmospheric scintillation has not previously been determined for 4 m telescopes, but the well known scaling law due to Young (1967, 1974) has been shown to work well at least at 2 to 2.5 m (GB92; KF92):

$$\text{scint}=0.09D^{-2/3}X^{1.75}\exp(-h/h_0)/\text{sqrt}(2t_{\text{int}}), \quad (11)$$

where D is the aperture diameter in cm, X is the airmass, h is altitude relative to a scale height h_0 of 8000 m and t_{int} is the exposure time in seconds. Young (1992) has pointed out an error in the GB92 paper of replacing Δf with $1/t_{\text{int}}$; the correct replacement is shown in Eq. (11). This changes our earlier (GB92) conclusion from having set a limit for scintillation some 20% below the prediction of the standard equation to some 20% above. In any case, since the scintillation can easily vary by a factor of two over time scales of minutes and days, the agreement is excellent (Young 1992) and the conclusion about the expected contribution of scintillation to the total error budget is unchanged.

The brightest M67 ensemble stars were expected to have comparable contributions from atmospheric scintillation and Poisson statistics when averaged over a full 8–9 h observing window. In order to quantify the atmospheric scintillation a triplet of well isolated brighter stars in NGC 752 (H177: $V=10.19$, $B\text{-}V=0.48$, H185: $V=12.22$, $B\text{-}V=0.54$, H186: $V=10.19$, $B\text{-}V=0.94$, see Eggen 1963 for photometry and finding chart) was observed before M67 could be acquired. Near one airmass, and observed with the Corning 4-96 filter, the 10th magnitude NGC 752 stars

TABLE 10. Noise simulation, No. 27, KPNO, January 14.

Hour angle	Poisson	Scint	sky	Total	Observed
−4.6	212	371	90	437	498
−4	209	269	78	349	345
−3	201	185	69	282	323
−2	198	145	61	253	252
−1	198	127	53	241	234
0	198	123	38	236	265
+1	198	127	28	237	258
+2	198	145	33	248	265
+3	201	185	36	276	283
+4	209	269	40	343	293
+4.6	212	371	51	430	340

had expected Poisson fluctuations two times smaller than scintillation. These time series were reduced using the full ensemble normalization and time series processing techniques. With only two dominant stars this was not a robust ensemble, but with observations taken during stable conditions it was suitable for estimating the atmospheric scintillation contribution to the error budget. Time series noise contributions for Poisson statistics and sky background (smallest of the three) were directly estimated and subtracted; assuming that the residual noise was entirely due to atmospheric scintillation yielded an upper limit estimate for its actual contribution. Table 9 details scintillation estimates (in ppm per minute equivalent integration) for KPNO and CFHT (all were acquired at an airmass very close to unity). The atmospheric scintillation estimates for Kitt Peak on three different nights correlate well both with wind speed and with overall time series precisions for M67 as in Table 3. Short time series on NGC 752 from Palomar showed a drift of 20 to 40 pixels in the image center (acquired without use of an autoguider) and were not suitable for a robust scintillation estimate.

Shown in Table 10 is a time-dependent simulation of error contributions for star No. 27 as observed 1992 January 14 at the KPNO 4 m. The modeled and observed noise levels are remarkably similar, suggesting both that the error budget is understood and that the observations and subsequent reductions allowed precision at the level set by irreducible terms. (We, of course, chose a case with good agreement to present; there are some individual star-nights where the observed fluctuations exceed the simple three term prediction. The converse is not found, i.e., there are not examples of observations yielding smaller than modeled irreducible errors, a situation that could arise if the time series processing was removing "real" noise.)

In Table 10 the first column gives hour angle for M67 observations; maximum airmass is 2.43 at HA=4.6 h. "Poisson" is simply the rms fluctuations (in ppm) expected from the observed counts. Column 3 gives atmospheric scintillation contribution based on Eq. (11), while "sky" is the expected contribution to noise from CCD readout noise and sky summed over the appropriate aperture size [Eq. (10)]. Column 5 labeled "Total" is the incoherent sum of the three previous error terms. Column 6 marked "Observed" is a smoothed local rms representation

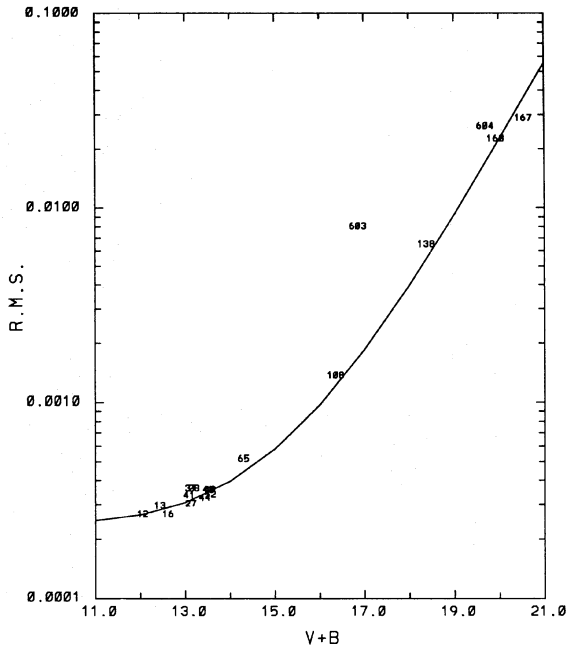

FIG. 8. Distribution of time series rms for the 18 stars brighter than 22nd magnitude for 1992 January 14 for Kitt Peak 4 m data. "$V+B$" indicates empirical magnitudes in the 4-96 filter system which happens to approximate the mean of these common passbands. Best stars are at ~250 ppm. Curve is empirical fit of atmospheric scintillation, target Poisson statistics and sky background error terms (all for conditions averaged over the full night). Star No. 603 is a close visual double with No. 13 and thus suffers from excess noise. Most points fall near a simple three component error budget curve suggesting that the relative photometry is limited by the expected irreducible terms.

obtained from the neighboring 30 points in the observed, fully processed relative intensity time series.

We have shown the distribution of noise over time for one star-night. The time-resolved error budget for a star of average brightness in Table 10 shows that Poisson and atmospheric contributions were comparable overall, but with atmospheric scintillation effectively imposing the limiting useful hour angle. Another way to examine the error budget is to plot the noise levels for separate stars for a given night as shown in Fig. 8. Again analysis of the error budget is simple and consistent with excellent control of time series precision.

Figure 9 shows details of the 1992 January 14 time series for star No. 16. This was the best night at KPNO, but conditions are not "photometric" as shown by fluctuations of a few percent, especially during the first 5 h.

Examples in which things did not work as hoped include 1992 January 17 (KPNO) in general and stars No. 13, 37, and 44 in particular. As noted in Table 9 there is evidence from immediately before the M67 sequence of unusually high atmospheric scintillation, perhaps consistent with high and gusty winds that night. This was also two nights before full moon so the sky was much brighter (but it was even brighter for the Palomar data on the 18th without causing undue problems). Despite considerable effort, no reliable explanation was found for the infrequent

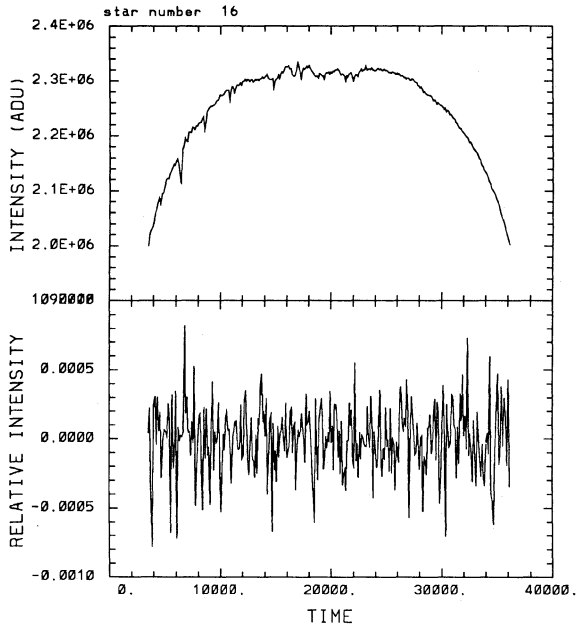

FIG. 9. Upper panel shows raw intensity (ADU) time series for star No. 16 as observed 1992 January 14 at KPNO. Lower panel shows relative intensity time series for the same case. Time is in seconds with an arbitrary zero point.

excess noise levels sometimes found on a few stars. The excess noise could not have been intrinsic as these same stars were well behaved simultaneously at other sites. On some nights, e.g., the 16th at KPNO, the seeing was near 4″ and variable, leading to much higher noise from image blending as discussed in Sec. *2.3*.

4.8 Final Time Series

How do the independent time series as processed by R.L.G. and H.K. compare? Can a significant gain be made by combining data from the two independent analyses sets? Table 11 compares measures of noise levels in our two analysis sets based on the mean amplitude level (ppm) from weighted discrete Fourier transform power spectra (approaches for the latter are described in Sec. *5.1*) over the 2.5–4.5 mHz frequency region, which is expected to be clear of any oscillations. Several points are immediately obvious from Table 11. The two independent time series analyses yielded very similar noise levels on average. An averaging of the two reduced time series results in lower noise, showing that both sets had "reduction" noise that was uncorrelated. (Noise from atmospheric scintillation or Poisson fluctuations is a *real* change of a star's measured intensity and should influence both series identically. Reduction noise refers to imperfections in the time series production.) On the other hand, the drop of combined amplitude is small compared to the drop that would have occurred if our two series were purely independent noise; our time series are highly correlated, as they should be.

TABLE 11. Comparison of H.K. and R.L.G. time series.

Star	HK amp	RLG amp	Combined amp	Fraction uncorrelated	Gain (%)
12	7.69	6.75	6.26	0.29	7.3
13	6.63	7.68	6.37	0.16	3.9
16	8.39	7.90	7.18	0.33	9.1
27	7.50	8.92	7.32	0.19	2.7
28	9.49	9.10	8.29	0.32	8.9
37	8.60	9.96	8.29	0.15	3.6
41	8.27	9.32	7.85	0.20	5.1
44	8.55	10.73	8.32	0.12	2.7
48	10.62	10.39	9.28	0.37	10.7
49	11.23	10.68	9.67	0.34	9.5
52	9.90	11.26	9.44	0.19	4.6
65	15.06	17.80	14.63	0.12	2.9

In Table 11, columns 2 and 3 labeled "H.K." and "R.L.G." correspond to mean amplitude (ppm) of 2.5–4.5 mHz region of separate power spectra. "Combined amp" is after a weighted average of the two time series. Column 5, labeled "Fraction uncorrelated" shows what part of the power is *not* in common between the two reductions {defined as [min(H.K.,R.L.G.)—combined]/[min(H.K., R.L.G.) $-1/(1/HK^2+1/R.L.G.^2)^{1/2}$], the last term giving combined amplitude had the two time series been unrelated}. "Gain" is percentage improvement of the combined amplitude relative to the min(H.K., R.L.G.). The average gain of the combined data set relative to the best individual set is $\sim 6\%$ (it would take 12% more data to make the same gain).

In all of the analyses and discussion to follow, unless otherwise noted, the combined time series from the independent work of R. L. G. and H. K. will be used. To illustrate the precision of our data and to set the stage for oscillation signal searches see Fig. 10 showing the combined time series for star No. 16. Although sobering to contemplate, it is worth pointing out that the oscillations we might hope to detect in this star (based on Table 1) have amplitudes of ~ 25 μmag and periods of ~ 1000 s; peak to peak this corresponds to the symbol heights and about $\frac{1}{6}$ their width. We are looking for signals quite obviously well buried in the noise, but we have a lot of data to work with, as well as the expectation that multiple modes in a single star have characteristics making their ensemble existence more easily recognized.

The distribution of relative weights [see Eq. (12) for use] for star No. 16 over the full time series is shown in Fig. 11. Weights are set as the inverse square of the time varying rms (after smoothing over about 1 h intervals). We have experimented with several options including no weighting, weights $\propto 1/\text{rms}$, $\propto 1/\text{rms}^2$ (as shown), and $\propto 1/\text{rms}^3$. Since the overall sensitivity to multimode oscillations depends not only on the mean noise level, but also the *extent* of nightly windows it seemed possible that the best sensitivity to detection of Sun-like oscillations would follow from a weighting function giving greater than inverse square contribution to the lower precision periods. Realistic simulations showed that the nominal $1/\sigma^2$ weighting worked best.

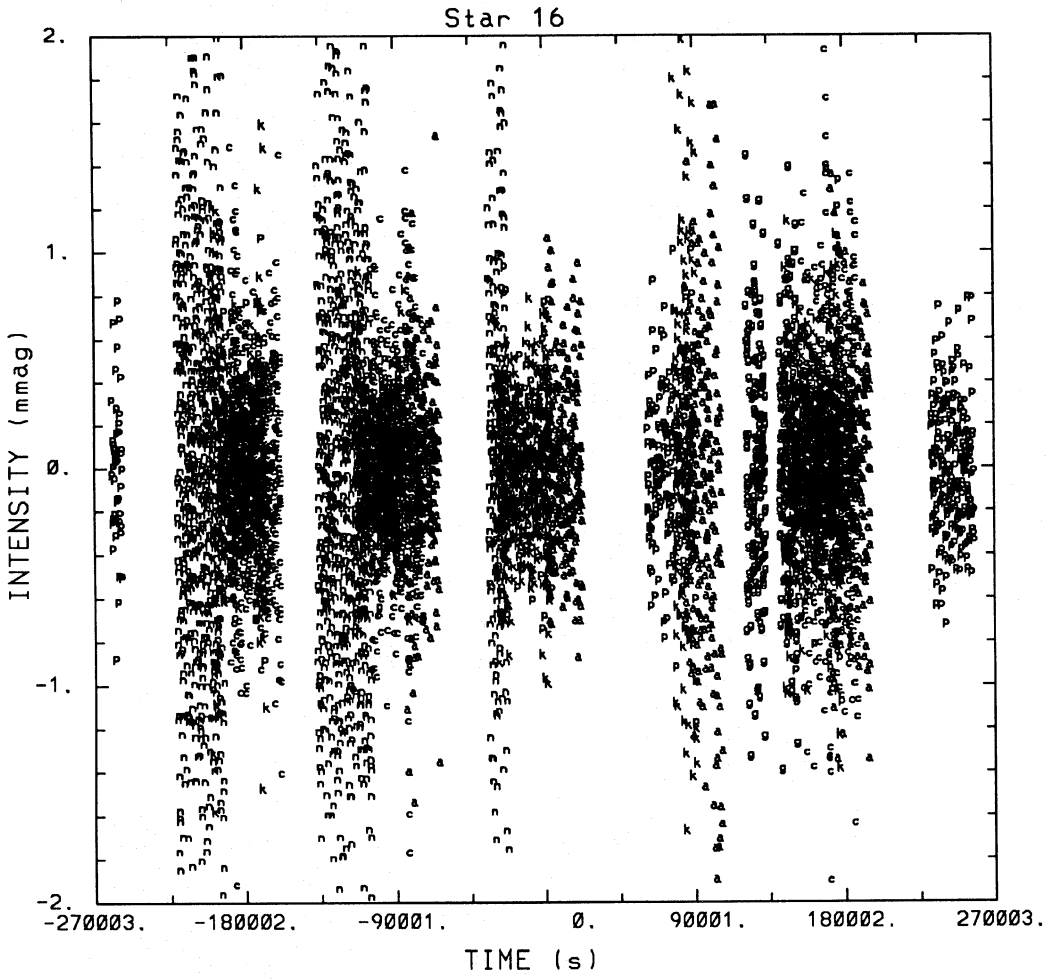

FIG. 10. Full network relative intensity time series amplitude in parts per thousand (~mmag) over the seven night period for star No. 16. Definition of symbols is: p=Palomar, n=NOT, f=CFHT, K=KPNO, a=AAT, c=CAA. This illustrates the good precision throughout and a window function much better than would follow from a single longitude site.

5. POWER SPECTRUM AND RELATED ANALYSES

Our data set has several common, but undesirable properties that complicate further analyses. The data points are not distributed uniformly in time; there are irregular and regular gaps of various sizes. This immediately rules out the use of Fast Fourier Transforms (FFT) for power spectra analyses, however, the discrete Fourier Transform, although much slower, is well posed and quite adequate for our purposes. The data points from different sites and times have quite different inherent noise levels, varying by over a factor of 3 in the mean. To optimally search for signals in our data we must take into account the different precisions through proper weighting of the data. There are some analysis steps that may be of only limited utility, e.g., CLEANing (Roberts *et al.* 1987), which can effectively remove side lobes of the window function, but which may result in greater statistical uncertainty about what the resulting spectrum represents. Whatever analysis steps are adopted, we must always run realistic simulations to test that signals are not found from analysis of data consisting of pure noise, but are correctly characterized if the simulation includes imposed signals.

5.1 Standard Analysis

In a previous search for stellar oscillations on Procyon, see Brown *et al.* (1991), we faced a distinctly different analysis problem. With the spectroscopic data on Procyon we had better signal-to-noise levels and excess power was clearly visible in a restricted part of the power spectrum domain. But the limited window function from observing Procyon at only one site did not provide sensitivity of the power spectrum of the power spectrum to expected frequency separations. The several nights of data on Procyon could be split into independent sets, with repeatability of structure in the power spectra yielding clues to the possible presence of coherent oscillations. In the present case we have very low expected signal to noise, but a sufficiently robust window function for power spectrum of power spectrum and folded spectra approaches to work well. We therefore concentrate in this work on the more direct ap-

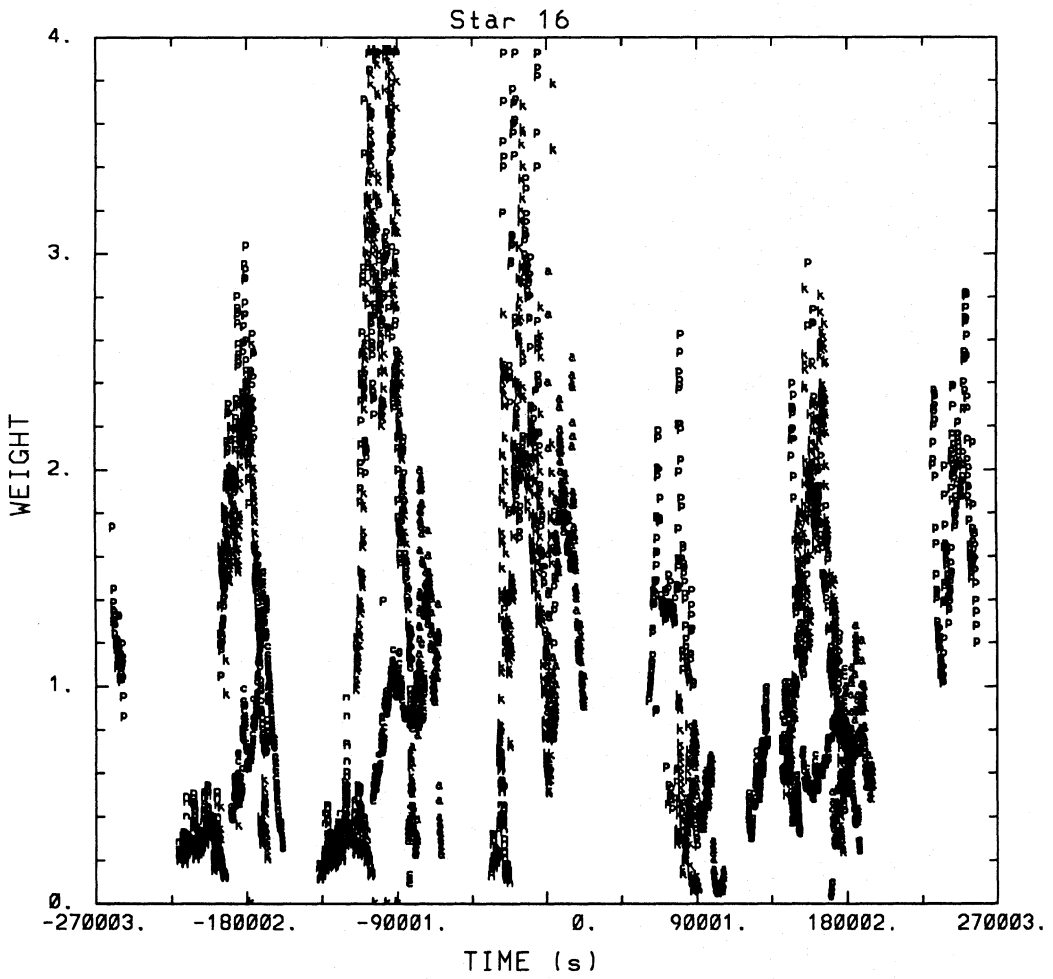

FIG. 11. Full network relative weights distribution. Symbols are as defined for Fig. 10.

proaches of power spectra, CLEANed spectra, power spectra of power spectra, and folded spectra as the primary analysis tools to be used in searching for oscillations in our time series.

We expect solar-like oscillations to be manifest as equally spaced peaks in frequency space (or a power spectrum) over a moderate domain. The Sun for example shows well defined peaks extending from 2500 to 3800 μHz (primary apparent spacing of 68 μHz) with largest amplitudes near 3100 μHz. This "picketfence" effect is likely to be the first recognizable signature of stellar oscillations from marginal data. To search for evenly spaced peaks in a power spectrum we may generate a power spectrum of the power spectrum (hereafter abbreviated as ps $\otimes$ ps) which would generate a peak at the primary frequency separation. (The ps $\otimes$ ps is generated using only a limited domain of the power spectrum centered upon the region being tested for the presence of oscillations.) But because the original power spectrum peaks are not sinusoids the ps $\otimes$ ps will also generate a series of overtones at the primary separation divided by 2,3,... . The ps $\otimes$ ps is a timelike function, so the fundamental and overtones plotted versus time will in turn be equally spaced. The ps $\otimes$ ps can be used to find weak periodic signatures in a power spectrum, but since it does not effectively localize this information, it is itself an imperfect tool. Furthermore the $l=0$ and 1 modes are not perfectly modeled by a simple $\Delta\nu_0/2$ spacing; this lack of coherence lowers the potential sensitivity of the ps $\otimes$ ps approach (see column 4 of Table 12). Another approach to searching for periodic signature in a power spectrum is to "fold" and average together successive segments of length equal to the periodic signature; we refer to this as simply a

TABLE 12. Theoretical frequency differences for star No. 27.

n	$\nu_{n,0}-\nu_{n-1,0}$	$\nu_{n,1}-\nu_{n-1,1}$	$\nu_{n,0}-0.5(\nu_{n,1}+\nu_{n-1,1})$	$\nu_{n,0}-\nu_{n-1,2}$
21	58.06	58.17	3.77	4.62
20	57.58	57.61	3.60	3.81
19	57.26	57.27	3.46	5.17
18	57.22	57.01	3.34	5.07
17	57.87	57.33	3.29	5.13
16	58.27	57.99	3.08	5.26
15	57.00	57.73	2.67	5.31
14	56.59	56.71	2.24	5.29

folded spectrum. Both of these approaches can be frustrated if the sought after signals are not perfectly periodic, but in fact show minor frequency-dependent variations in mode spacing. If instead of cutting a power spectrum in equal segments and averaging, we instead stack the segments one on top of another in a graphic display, we form an echelle diagram. Evenly spaced peaks in a power spectrum transformed into an echelle diagram follow straight lines, vertical if the cut length is correct, tilted if the cut length does not match the periodic structure. If the separation between features is itself a function of frequency, then the echelle diagram power ridges show curvature. Use of echelle diagrams is generally warranted only when the signal to noise is high enough to easily see individual modes; this is not the case for our data sets. The solar p-mode echelle diagram shows significant curvature and the same may be expected for other stars.

To sum up: we seek evidence of evenly spaced structure in power spectra, but the multiple peaks may not have coherent spacing over their full domain.

Entries in Table 12 follow from the theoretical eigenfrequencies presented in Table 4 of GB92. The mean values of $\nu_{n,0}-0.5(\nu_{n,1}+\nu_{n-1,1})$ (also referred to below as $l=0$ and 1 offset) are consistent with the asymptotic relation given as Eq. (1) with $A\sim 30$ μHz, but the trend does not match the simple asymptotic relation. [To explain the $l=0$ and 1 offsets A in Eq. (1) would have to vary smoothly from 16 to 41 μHz over $n=14$ to 21, while $A\sim 15$ μHz would provide a match to the $l=0$, 2 splitting independent of frequency. A similar table formed from solar frequencies would show similar anomalies relative to the asymptotic relation. In particular the splittings $l=0$, 1 and 0, 2 are less variable with frequency than a constant value of A in Eq. (1) suggests.] In theoretical discussions of the asymptotic formula [Eq. (1)] differences of frequencies as shown in Eq. (2) are routinely invoked as the means by which core structure might be probed. Since the relative offset of $l=0$ and 1 modes is more likely to be detectable from low signal-to-noise observations, it would be valuable for future theoretical studies to investigate how stellar structure might be constrained by this quantity alone. For the other representative stars with reliable models our theoretical results (GB92) show $l=0$ and 1 offsets of 3.61 (No. 28), 0.2 (No. 37), and 4.40 (No. 48) μHz.

We will often refer to amplitude spectra. These are formed very simply as the square root of power at each frequency and are in some cases the most convenient way of displaying either the direct or CLEANed power spectra.

Having described in overview the tools we will use, let us now give details of deriving "weighted power spectra," since this is a nonstandard approach. Unlike FFTs, discrete Fourier Transforms can be evaluated at any desired frequency and there is good reason in general to do so on an oversampled grid ($\Delta\nu \ll 1/T$, where $\Delta\nu$ is frequency sampling of transform and T is the data set length). Scargle (1982) has demonstrated the equivalence of sine and cosine fitting with Fourier transform based power spectral analysis. Expressed as linear fits of sines and cosines, adoption of unequal weighting is straightforward.

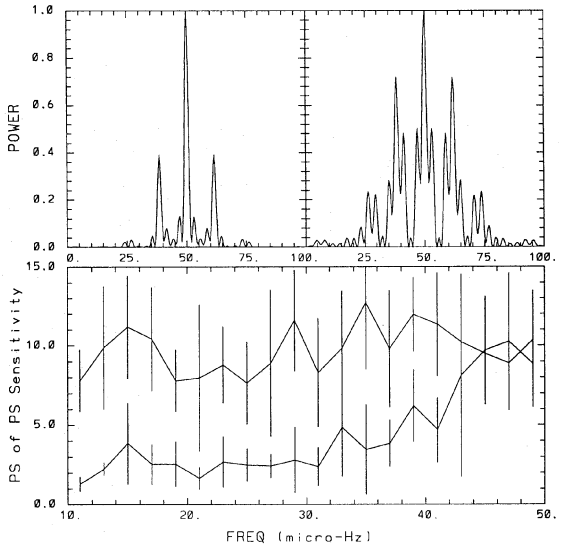

FIG. 12. Upper panels compare window function for full network (left) generated as the (weighted as for star No. 16) power spectrum of a pure sinusoid with a period of 1000 s (plotted vs an arbitrary center of 50 μHz) with that for the Palomar data alone as representative of observations from a single site. Lower panel compares the ps $\otimes$ ps response function vs $\Delta\nu_0/2$ as defined in the text for the realized network campaign with the response function for a data set of similar total noise level, but restricted to one longitude site (lower curve). Error bars show $\pm 1\sigma$ deviations from 10 independent realizations.

One of us (R.L.G.) has adopted the following.

Assume the unevenly spaced data are represented as d_i, $i=1,N$ for which weights, w_i, $i=1,N$ have been defined for all times t_i, $i=1,N$. Assume that we wish a Fourier-like decomposition at frequency separations $\Delta\nu=0.25$ μHz to oversample our 6 day domain by a factor of about 10 over $\nu=0.25$ to 5000 μHz, then for all $\omega=-j2\pi\Delta\nu$ ($j=1$, $M=20\,000$ for current example) evaluate

$$a_j=\sum_{i=1}^{N} w_i d_i \sin(\omega_j t_i) \Big/ \sum_{i=1}^{N} w_i, \tag{12}$$

$$b_j=\sum_{i=1}^{N} w_i d_i \cos(\omega_j t_i) \Big/ \sum_{i=1}^{N} w_i. \tag{13}$$

The a_j, b_j and their complementary window function obtained by setting $d_i=1.0$ everywhere may be passed to the CLEAN (Roberts *et al.* 1987) process, or immediately transformed to a power spectrum as

$$p_j=a_j^2+b_j^2 \tag{14}$$

or the equivalent amplitude spectrum as

$$\mathrm{amp}_j=p_j^{1/2} \tag{15}$$

at all j to cover the desired frequency interval. To obtain properly amplitude calibrated spectra we simply scale amp_j, or p_j, as necessary to obtain the correct level for test sinusoids of specified amplitude.

A measure of network coverage completeness is provided by the window function as shown for star No. 16 in Figure 12. Since we are utilizing weighted power spectra

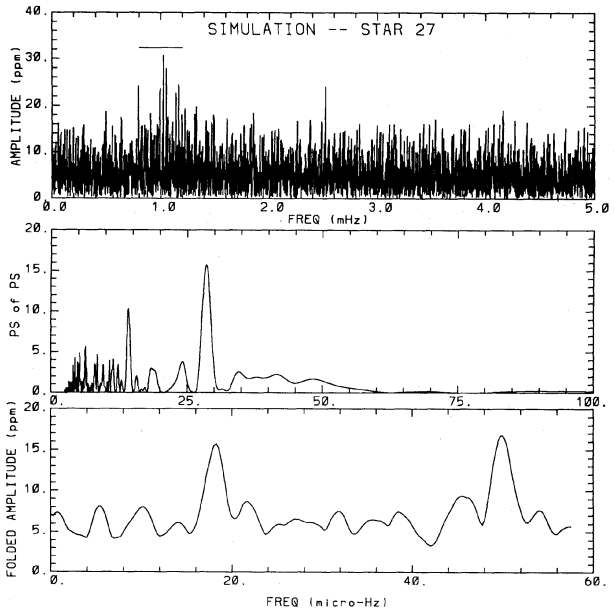

FIG. 13. Simulation results with imposed signal at peak amplitude of 30 ppm. Upper panel shows CLEANed amplitude spectrum (bar shows frequency window used for computation of the ps ⊗ ps). Middle panel shows ps ⊗ ps in which imposed signal with $\Delta\nu_0/2 = 28.8$ μHz is obvious. Lower panel shows folded (at $\Delta\nu_0$) amplitude spectrum from which the known input mode locations can be easily recognized.

there are minor differences on a star-by-star basis. Side lobes at 11.6 μHz for one over a day aliasing are prominent, but significantly reduced over what a single site would provide. The ratio of central to side lobe power provided by our window function supports CLEANing quite well. Another measure of the window function, perhaps more relevant to the detection of low signal-to-noise solar-like oscillations, is how well evenly spaced peaks can be picked out with a ps ⊗ ps analysis. For the ps ⊗ ps response curve in Fig. 12 we have done the following: (1) Take a realization of noise and weights matching well the real data distributions shown in Figs. 10 and 11. (2) Take the eigenfrequencies used to model star No. 27 (GB92) and scale as necessary to generate $\Delta\nu_0/2 = 13,15,...,45$ μHz. (3) At each assumed $\Delta\nu_0/2$ generate a simulation (see next paragraph) at peak amplitude of 30 ppm. (4) Generate a power spectrum, CLEANed power spectrum and, using a window scaled to just span the signal, extract the ps ⊗ ps for each simulation. (5) Evaluate the ps ⊗ ps peak at the imposed $\Delta\nu_0/2$ and divide by the mean ps ⊗ ps level over 3–100 μHz. This is the quantity plotted as the ps ⊗ ps response function in Fig. 12. Also shown in Fig. 12 is the ps ⊗ ps response function that would follow from just the Palomar data with noise reduced by a factor of 2.5, as an indication of what equivalent observations would yield if not supplied by a longitude distributed network. In the domain of 17–35 μHz a single site provides a formal ps ⊗ ps equal to zero if the direct power spectrum is used. CLEANed data provides small sensitivity and general noise in this domain even from a single site, but only with a better overall window function does the ps ⊗ ps response become useful over the full derived frequency range.

We show in Fig. 13 several of our standard tools for detecting solar-like oscillations in the context of a simulation with known input signals. Since our quoted sensitivity levels for detection of, or upper limits on, solar-like oscillations depend in some detail upon how we set up the simulations, we must describe our approach. A realistic simulation is first set up with a distribution of white (Gaussian distributed) noise at the same observation times as the real data *and* with a distribution of rms that tracks that existing in the real data. Although point by point they would be independent, a plot of the simulation data used for Fig. 13 would appear equivalent in general morphological terms to that for the real time series shown in Fig. 10. (The latter statement holds true even with superimposed signals, since such are at small amplitudes compared to the noise level.) To the base of simulated noise we may add a simulated signal. For solar-like oscillations we have chosen to use a distribution of eigenfrequencies taken from stellar evolution models of the M67 ensemble (GB92). The particular case of star No. 27 was given as Table 4 in GB92. Amplitudes for the simulation are specified by some quoted peak value that applies to the $l=0$ mode closest to ν_{pk} of Table 1. Mode amplitudes are scaled as 0.9, 0.5, and 0.1 at $l=1$, 2, and 3, respectively. Amplitudes are also prescribed to decline smoothly away from the central n (0.8, 0.64, 0.51, 0.4 symmetrically for $\Delta n = 1$, 2, 3, and 4). All phases are assigned randomly. This provides a reasonable simulation of the long-term average of solar oscillations. The above is how the parameters governing most of our simulations, and in particular that for Fig. 13, have been set. Observations of the Sun over different six day windows will show the same modes fading in and out at the same frequencies, but with unique phases and amplitudes in separate sets. In any six day window the distribution of amplitudes will roughly conserve total power, but have randomly distributed amplitudes. We will in a few cases compare simulation results using randomly distributed amplitudes.

Other approaches [than Eqs. (12)–(15)] to generating a power spectrum may be used. Eqs. (12)–(15) represent a least-squares based noise filtering. One of us (H.K.) has formed power spectra using the following approach: (1) For each frequency at which the power is to be evaluated transform the time series into a folded time series (magnitudes as a function of phase). (2) Fit the data to a phased sine function using statistical weights from the time series analysis. (3) Give low weight to non-sinelike solutions. We have found it possible to reduce the noise in the power by 20% without changing the amplitude of real signals (synthetic oscillations used as tests). As an example this approach yields a 2.5–4.5 mHz noise level of 6.6 ppm for star No. 27 compared with 7.3 ppm as given in Table 11.

H. K. has also pursued a direct fitting method (referred to later as: "comb analysis") to analyze the discrete (not CLEANed) power spectra for evidence of equally spaced peaks. This method is described in Kjeldsen (1993b). The precise sequence is as follows: (1) For a given assumed $\Delta\nu_0$ fold the power spectrum within a window centered on the

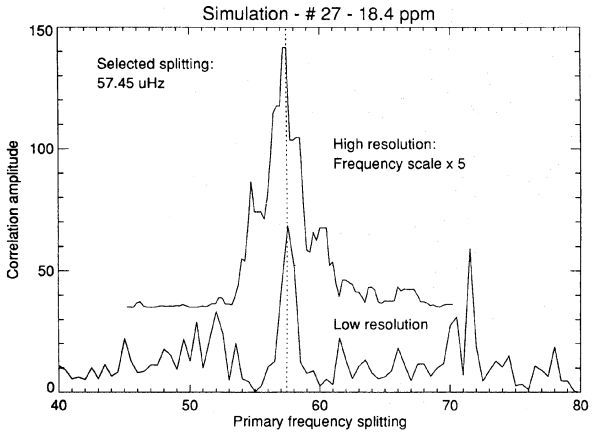

FIG. 14. Comb analysis (H. K.) as applied to a simulated direct amplitude spectrum for star No. 27. Lower curve shows the correlation amplitude vs test values of $\Delta\nu_0$ over 40–80 μHz. The upper curve shows the same, but on a finer search grid over 55–60 μHz. Dotted line shows position of known mode separations.

assumed peak power with a set of Gaussian peaks (distance between peaks: $\Delta\nu_0$) having the following amplitude (in power) distribution: 0.4, 0.7, 1.0, 1.0, 1.0, 0.7, 0.4. To allow for slight mode curvature each peak is allowed to move ± 2 μHz, however a weight function lowers the contribution in proportion to the distance a peak moves. (2) Fit a second set of peaks with separation $\Delta\nu_0$, but at an offset of $\Delta\nu_0/2$ within an allowed range of $\pm\Delta\nu_0/4$. This should identify the complementary $l=0$ or $l=1$ mode set. (3) Repeat steps (1) and (2) over a grid of assumed peak power location mapping out all possible locations of peaks

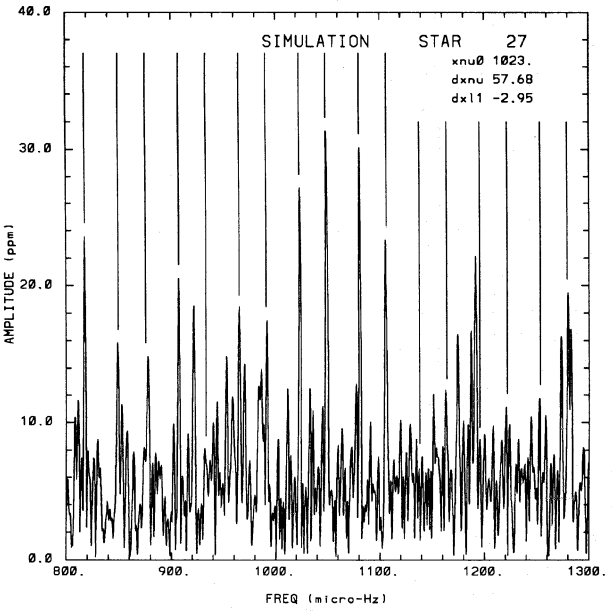

FIG. 15. Comb analysis (R. L. G.) as applied to a CLEANed simulated amplitude spectrum for star No. 27 [see Eqs. (16) and (17)]. Curve shows real spectrum, vertical lines mark positions of lines given by the asymptotic formula fit.

TABLE 13. CLEANed amplitude spectra statistics.

	Amp ppm	Max(amp) ppm	Max/mean	Max(amp) ppm	Freq. μHz	Max/mean
Star	2.5–4.5mHz			0–5mHz		
12	4.77	18.6	3.9	24.9	99	5.3
13	5.03	18.9	3.8	23.8	466	4.7
16	5.55	22.4	4.0	29.0	696	5.2
27	5.69	21.7	3.8	23.5	1336	4.1
28	6.50	22.6	3.5	22.6	276	3.5
37	6.43	26.3	4.1	26.3	3272	4.1
41	6.11	26.7	4.5	27.3	1256	4.5
44	6.67	25.9	3.9	33.3	1464	5.0
48	7.35	27.6	3.8	29.2	1031	4.0
49	7.42	30.4	4.1	41.2	631	5.6
52	7.05	30.1	4.3	32.7	526	4.6
65	10.6	44.9	4.3	48.8	2024	4.6

with such separations in the power spectra. (4) Evaluate the overall best fit to the power spectrum, and give a value of the quality of this fit based on the amplitude of correlation. (5) Repeat steps (1)–(4) over a range of assumed $\Delta\nu_0$. The optimized solution will, for each splitting, give best values for peak power location, amplitude at maximum, and the displacement of $l=0$ and 1 peaks. At input peak amplitudes for star No. 27 of 20 μmag this process yields a reliable, clear signal detection and all $l=0$ and 1 modes with n within ± 2 of the peak are detected within ± 2 μHz. Figure 14 shows the correlation amplitude for the star No. 27 simulation using this technique. Even with peak amplitude at only 18.4 ppm the correct signal is easily recognized (see Kjeldsen 1993b).

R.L.G. has pursued related comb analyses, but applied to CLEANed spectra. Figure 15 shows a comb analysis solution to a simulation for star No. 27 in which an asymptotic relation [similar to Eq. (1)] is used to define all the frequencies:

$$\nu_{n,0}=xnu0+dxnu(\Delta n), \tag{16}$$

$$\nu_{n,1}=xnu0+dxnu(\Delta n+1/2)+dxl1, \tag{17}$$

where to match the simulation Δn ranges over ± 4. A solution for the three variables is obtained using the downhill simplex method (Press *et al.* 1992) to minimize the overall residuals after performing a linear least-squares fit of the window function at each of the specified frequences as in Eqs. (16) and (17). The offset between $l=0$ and 1 modes (see Table 12) is easily seen in Fig. 15. This approach also provides a linear least squares based amplitude estimate for the mode at each specified frequency, although at our low S/N these individual mode estimates are not reliable. At simulation levels of 20 ppm peak amplitude this approach provides stable solutions even though the individual modes are not obvious above noise in the CLEANed amplitude spectra. To assess significance of signals found in either the ps $\otimes$ ps or comb analyses we rely on comparison with large ensembles of null experiments. In particular for each ps $\otimes$ ps peak considered as indicative of a stellar signal we determine how often the identical analysis would produce as large a peak starting with independent noise realiza-

tions. We make the same comparison with a large number of random scramblings (keeping observation times but randomly exchanging the data and weights). Similarly with the comb analyses we determine how often the asymptotic form indicated by the stellar data results in fits as good or better from null experiment data.

5.2 Upper Limits to Oscillation Amplitudes

A good general overview of attained sensitivity to oscillations can be provided with a discussion of coherent power spectra statistics for each of the ensemble stars. Table 13 gives details of noise levels in amplitude spectra after CLEANing (Roberts *et al.* 1987). Comparison with Table 11 shows that the noise level in the dirty amplitude spectra is about 30% higher. This does not necessarily imply that the process of CLEANing has increased the sensitivity by a corresponding amount; we again emphasize that we rely on self-consistent empirical calibrations of amplitudes to establish sensitivities. To use CLEANed spectrum statistics, our conclusions must be formed on the basis of many simulations using the same processing.

Columns 2–4 of Table 13 refer to the frequency domain of 2.5–4.5 mHz expected to be oscillation free and to be well away from any $1/f$ noise or effects of temporal filtering. The highest peaks in the domain of 2.5–4.5 mHz are typically 4σ above the mean, as expected for the number of data points. The last three columns give overall peak amplitudes, their position and the ratio to the mean amplitude of column 2. Highest peaks remain at the level of $4-5\sigma$, i.e., no coherent oscillations are immediately obvious above the general noise level from inspection of the power spectra.

There is a tendency for the highest peak in the amplitude spectra to occur near the projections given in Table 1, i.e., stars Nos. 12, 16, 27, 44, 48, and 65 are in good agreement. Only star No. 12 has expected peak oscillation amplitudes in the domain affected strongly by both $1/f$ noise and our temporal filter; it will be further discussed in Sec. *6.12*.

Assuming that any oscillations with peak amplitudes near the highest peaks in the CLEANed amplitude spectra are solar-like, we can improve the sensitivity by testing for multiple modes evenly spaced in frequency. Figure 13 showed a realistic simulation for star No. 27 with a peak amplitude of 30 ppm. The simulated signal is obvious in all of the panels, especially so in the ps ⊗ ps and folded spectrum. From many such simulations it is clear that signals at a peak amplitude greater than $5\times$ the mean amplitude spectrum level (column 2 of Table 11) would be *unambiguous*—no such signals are present in stars No. 13 through 65. For star No. 13 we thus claim sensitivity to oscillations at $5\times 5.03=25$ ppm; this is close to the lower range quoted in Table 1. Similarly for star No. 16 we would expect to have unambiguous sensitivity to oscillations at 28 ppm, again this is very close to the lower range of projections. [Note that GB92 using a less precise interpolation in temperature and luminosity representing the Christensen Dalsgaard & Frandsen (1983) theory gave higher projections for stars 13 and 16, for which the lower range exceeded the observed upper limits. Current comparisons utilize Eq. (4).] Other stars for which upper limits fall within the range specified in Table 1 are Nos. 27, 37, and 41, while for the remaining stars the upper limits for *unambiguous* detection remain above the range of expectation. Our upper limits have reached the domain of some interest to theory, but are not in any case smaller than the currently projected lower range for stellar oscillations. (Note however that, somewhat surprisingly, the solar amplitude remains uncertain; should the upper range of claimed solar photometric oscillation amplitudes prove correct our upper limits would be of still greater interest.) Our analysis path to arrive at upper limits is admittedly a long and tortuous one including a complicated ensemble normalization and time series processing stage, a simulation involving model eigenfrequencies with an assumption about mode amplitude distribution, and a power spectrum of power spectrum analysis step.

What factors, if addressed in different ways, would influence our conclusions about mode amplitude upper limits, and by how much? The most important factor is our specific choice concerning mode amplitude distribution via scaling from solar oscillation properties. Our model input modes include a full n range of nine with a half power full width of $\Delta n=3$ corresponding to a frequency domain of less than 200 μHz for the subgiants (Nos. 27 and 41). The results of Brown *et al.* (1991) for Procyon, a star closer in spectral type to the M67 subgiants than is the Sun, suggest a half power width of perhaps 800 μHz centered at nearly the same peak amplitude as our predictions. Were we to put in a much broader distribution of power (i.e., more modes) this would certainly lower our claimed sensitivity level for upper limits. Naively the increase of a factor of four in number of modes would lead to a full factor of two improvement, but this would only follow if the modes maintain equal spacing over the full domain if a simple ps ⊗ ps or folded spectrum analysis is relied upon. On balance our assumption of the number of modes to include was probably too conservative and from this factor alone we could argue for upper limits lower by a factor of 1.5 to 2.0. Mitigating against lower values, however, was our optimistically smooth distribution of amplitudes for the modes we did include. The ps ⊗ ps responds best to a dense grid of periodic structures; if the amplitudes are greatly different mode to mode the sensitivity drops. Instead of scaling mode amplitudes at n and l to values based on the long-term envelope for the Sun, we have run simulations in which, for any given mode, its amplitude is scaled by a Gaussian distribution. This is probably a better representation of solar amplitude distributions, but is it really better for the M67 stars? We do not believe that the Procyon data shed any light on this point. In any case this approach leads to sensitivity of about 25% less on average, that is if our standard simulation just begins to reliably show oscillations present at 25 ppm, then simulations with randomly variable amplitudes would, on average, require 31 ppm to be as detectable. This latter point should be taken to indicate general uncertainty about how to reliably set upper

limits, but it should not be used to extend the upper limits of 25 ppm on star No. 13 or 28 ppm on star No. 16 upward by an additional 25%—these upper limits already correspond to the highest peaks present in the real power spectra which can be taken as reliable upper limits.

To sum up the discussion of upper limits on possible oscillations in the ensemble stars:

(1) We have performed simulations that are reasonable, and on balance are on the conservative side.

(2) The derived upper limits are in many cases within the range projected for oscillations and in some cases very near the (conservative) lower projection.

(3) A robust simulation of sensitivity to stellar oscillations requires more information about the nature of the oscillations than we currently possess.

(4) The allowed range of upper limits to oscillations runs from about three to five times the mean amplitude spectrum level shown in Table 13; our values to be quoted in discussion are based on the more conservative ($5\times$) limit.

A null result in detecting *unambiguous* evidence for the existence of stellar oscillations in a given data set should not be taken as the final analysis step. We argued, based on our standard analysis—maybe conservative overall—that simulations with signals at five times the mean noise levels would be unambiguous. But at what amplitude level would we usually expect to see evidence of oscillations in the ps $\otimes$ ps? From standard simulations it is clear that oscillations at about four times the mean amplitude spectrum level would be noticeable. That is, if we compute a large number of independent noise and signal realizations at this level, greater than 90% of the time the expected ps $\otimes$ ps peak will be locally highest. *But searching for signals "buried in the noise" is fraught with the danger of overinterpretation!* We should always consider the negative possibility and ask the question: Can what we observe be explained as an effect of noise alone. If we blindly take power spectra of power spectra over arbitrary domains, and *try* to find interesting peaks, then we would be virtually guaranteed of "success." Thus any claims for detections that we may be able to pull out of our data cannot be made with great certainty. The approach of fitting evenly spaced peaks (comb analysis) to the data may provide an even better sensitivity level, but will also suffer from significance that is difficult to quantify. Keeping these important caveats in mind, can we nonetheless develop arguments supporting the presence of oscillations? Addressing this question for each of our ensemble stars in turn will be the topic of Sec. 6.

5.3 Comparison with Previous Studies

A recent, thorough comparison of high-precision photometry results was provided in KF92. We compare our results here with the three previous best results measured in terms of estimated noise in the amplitude spectrum at high frequency (3 mHz). The two best previous photometric campaigns were directed toward detailed study of δ Scuti and roAp stars, for which very lengthy observing runs at high precision were required for adequate frequency resolution and detection of (by normal standards) low amplitude modes.

The most precise result in the literature, Kurtz *et al.* (1989), follows from some 580 h of observations with 1 m class telescopes on the oscillating Ap star HR 1217 using single-channel photoelectric photometry. Their observing run involved the collaboration of eight sites, the most intensive part of which was centered around a five-week grant of continuous observing time on the SAAO 1.0 m telescope. The estimated amplitude spectrum noise level at 3 mHz was 20 μmag (KF92). Table 11 of this paper (column 4, the combined amplitude of H.K. and R.L.G. averaged results) may be compared directly (after multiplying by 1.085 to convert our ppm to μmag). The best star in our ensemble has a noise level of 6.74 μmag (6.21 ppm) and is therefore 3 times less than the level of that observed by Kurtz *et al.* (1989). Our faintest ensemble star (No. 65) is still a factor of 1.3 better than the photoelectric photometry result. If we average the latter "advantage" factor over all 12 ensemble stars the result is 2.26. Since we surveyed 12 times as many stars, it is reasonable to quote a multiplexed improvement over the best previous single-star results of $\times 27$. It should be noted of course that the Kurtz *et al.* (1989) observations of HR 1217 were very successful in quantifying six principal oscillation modes and numerous rotationally split components with amplitudes ranging from 150 to 1050 μmag. The rich oscillation spectrum detected in HR 1217 provided one of the best initial successes for asteroseismology, allowing significant physical interpretation related to the complicated structure of this magnetic Ap star.

A three-channel photoelectric photometry campaign (Belmonte *et al.* 1990; Mangeney *et al.* 1991) using some 185 h of observations on two 1.5 m telescopes provides the second best results in terms of overall noise level. This two-site campaign followed the δ Scuti star 63 Her using the F2 V star HD 155543 as a comparison. This campaign attained a high frequency amplitude spectrum noise level of ~ 30 μmag. Our best results from Table 11 are 4.5 times better than the above result while the multiplexed advantage (comparing with two stars now) is $\times 20$. Again this was a very successful asteroseismology program supporting a physical discussion of the δ Scuti star (Mangeney *et al.* 1991). Of more direct interest for this campaign are the limits on and evidence for oscillations in the F2 V star with a luminosity and temperature close to star No. 28 of our ensemble. Applying the conservative approach of Sec. *5.2* would allow an *unambiguous* upper limit of about 110 μmag for solar-like oscillations to be placed on HD 155543. Based on the relative noise levels at 3 mHz our sensitivity for star No. 28 is 3.3 times better than the result for HD 155543. The photoelectric photometry, however, shows increased $1/f$ noise almost double that at 1.5 mHz where the oscillation peak is expected, while the CCD ensemble photometry produces a flat noise spectrum over 1–4 mHz. The relative improvement in sensitivity on single stars relative to this best previous photometric result on an F star is realistically a factor of at least 5. Given the in-

vestment of a comparable amount of observing time, but on 4 m versus 1.5 m telescopes, and with use of a more robust ensemble normalization, this level of improvement is expected.

The third best noise level attained previously was with the 0.9 m telescope, CCD ensemble photometry based observations of M67 (G91). Although a 3 mHz noise level of $\sim$45 μmag was attained, these observations from a single longitude provided sensitivity to solar-like oscillations at least 10 times poorer than with the current experiment. Given a comparable number of stars at the high precision level in the current and G91 experiments the multiplexed advantage is also a factor of 10. Gilliland *et al.* (1991) presented in their Fig. 17 "best-case" evidence for solar-like oscillations in four ensemble stars, one of which (No. 37) is also in the present ensemble. Interpreted as solar-like oscillations the ps $\otimes$ ps peak shown in Fig. 17 of G91 would require peak oscillation amplitudes of 100 to 150 μmag. Such oscillations would be dramatically obvious in the current data set. Fortunately, it was noted in G91 that: (1) "Should the suggestion of real *p*-mode oscillations from this study be real, then small improvements would yield an unambiguous detection." (2) "We believe that we have only seen noise fluctuations, that examined with enough optimism, resemble expected signals, and that real oscillations have not been detected." It is now clear, as was then suggested by detailed simulations, that the previous suggestion of oscillations did arise only from noise. The problem next at hand is to fairly present the evidence for oscillations that appear in analyses of the current, much richer, data set, *and* to again offer our best judgement as to the reality of any suggestions that solar-like oscillations are detected.

6. BEST EVIDENCE FOR COHERENT *p*-MODE OSCILLATIONS

In this section we will attempt to build the best possible case for the existence of stellar oscillations. Pursued without a skeptical attitude this would be a rather meaningless exercise. Claims of clear detections in this and other fields of science based on less evidence than we will present below are not uncommon. With a data set as rich as ours it would be quite easy to pick out coincidences of certain peaks and build a "case" for detection. Recognizing that this is a far too easy trap to fall into is not a good reason to not proceed, but we urge the reader to consider the remainder of this section in the following spirit: This project used a substantial community resource, and we have an obligation to analyze the resulting data as fully as possible. After presenting "the best possible case" we will offer an assessment of its significance based on our general experience and from analyzing simulations of a general and specific nature.

The most complete discussion is provided for stars Nos. 16 and 27 that show the clearest evidence for stellar oscillations. Stars Nos. 12, 28, 37, and 41 show significant evidence for signals. Some of the remaining stars also yield suggestive results, but will not be discussed in as much depth since we do not believe a good case can be made for detection. In order to simplify the ensuing discussion we present the stars in a generally decreasing order of interest keeping like spectral types grouped in sequence.

TABLE 14. ps $\oplus$ ps summary star No. 16.

ν_{cent}	ν_{fund}	$\nu_{harmonic}$
700	17.3	8.9
800	19.9	9.6
900	19.3	9.9
1000	19.2	9.5
1100	19.2	...
1200	18.8	9.5
1300	18.1	9.5
1400	17.9	9.6
1500	18.0	9.3
1600	...	9.3
1700	19.4	9.6

The star-by-star discussion to follow will present evidence for near, or marginally significant, detection of stellar oscillations for a broad range of both subgiants and main-sequence objects. The significance levels derived depend on the range of peak separations that we are willing to consider. This range is set by the theoretical splitting expected, combined with the confidence (or lack thereof) in the models that produce them. Section 8 contains a discussion that should be considered before passing final judgement on the detailed results presented next.

6.1 Star No. 16

The theoretical predictions for this star can be called into question. The star's HR diagram position lies about 0.5 mag above the nominal subgiant branch, so a simple stellar model consistent with M67 properties does not pass through the observed location. The mass and oscillation frequency separations quoted in Table 1 are consistent with the HR diagram position being explained as the sum of two similar component stars, while the projected position and amplitude of peak oscillations are consistent with the (more optimistic for these purposes) assumption that the implied luminosity and temperature apply to a single star. Quantitative knowledge of stellar oscillation frequencies would be very valuable for interpreting the structure of stars such as No. 16. If we assume No. 16 is a single star, the oscillation frequency separations, $\Delta\nu_0/2$ and $\Delta\nu_{20}$ should scale as $M^{1/2}R^{-3/2}$ [Eq. (2)], which compared with results for stars 27 and 41 (assume $\mathcal{M}/\mathcal{M}_\odot = 1.4$ for No. 16), would imply values of $\sim$19.9 and 3.5 μHz, respectively. The radial velocity study by Mathieu & Latham (1986) yields ambiguous results for this star (S984), the formal radial velocity dispersion is higher than expected for a single star, but formal classification as a binary depends on whether or not the most discrepant point (of 13) is retained.

Power spectra of power spectra for this star show interesting evidence of solar-like stellar oscillations. Table 14 details the most suggestive peaks that appear in searching many ps $\otimes$ ps for this star. A standard analysis set for star No. 16 is shown as Fig. 16 (window centered at 1000 μHz,

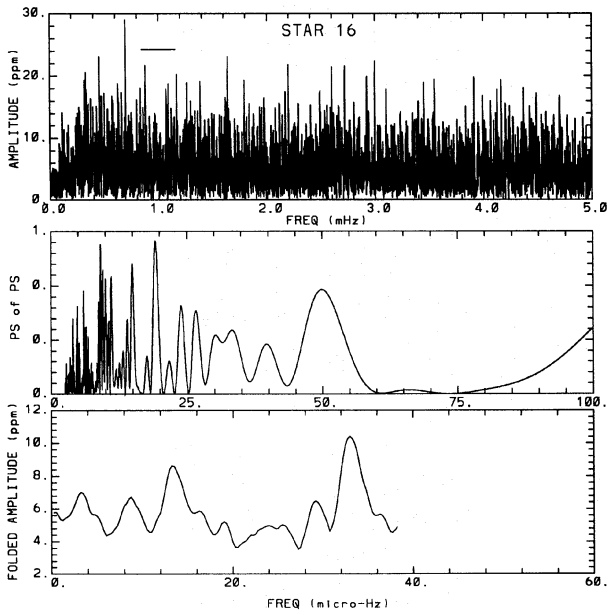

FIG. 16. Same standard analysis set as Figure 13, but for real data on star No. 16.

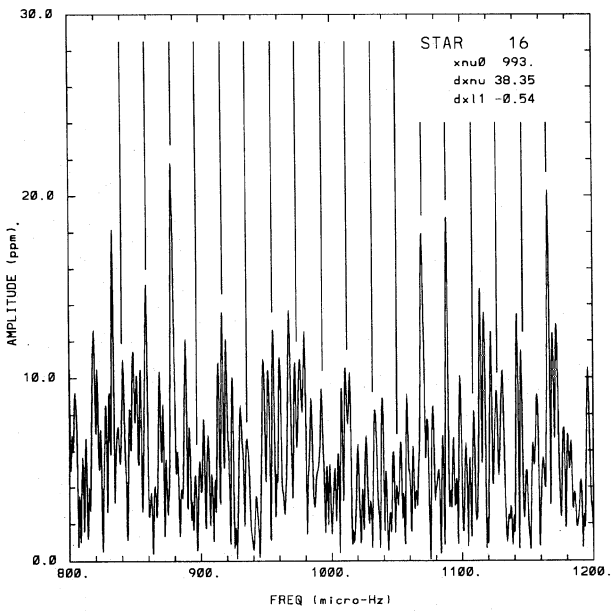

FIG. 17. Comb analysis as applied to real data for star No. 16.

fold length $\Delta\nu_0 = 38.25$ μHz; the corresponding entry in Table 14 is $\nu_{cent} = 1000$). The ps $\otimes$ ps use 310 μHz bands centered as shown by ν_{cent} and reveal evidence for a signal with $\Delta\nu_0/2 \sim 19$ μHz. If these reflect real solar-like oscillations with a mode-amplitude distribution like that detailed in Sec. *5.2*, then the ps $\otimes$ ps peak heights centered near 1100 μHz are consistent with peak oscillation amplitudes of ~ 20 μmag (or 18.5 ppm—although in this paper we distinguish between μmag and ppm, in practice the intrinsic uncertainty is larger than this difference). Note that in Table 14 every third line is essentially independent given the 310 μHz bands adopted for the ps $\otimes$ ps. The variation of ν_{fund} with frequency as seen in the ps $\otimes$ ps is comparable to what might be expected theoretically for $\Delta\nu_0/2$. The implied mode curvature (see Sec. *5.2* discussion) is sufficient to prevent wider ps $\otimes$ ps bands from being used to improve sensitivity.

The columns of Table 14 are as follow: ν_{cent} is the center of the power spectrum frequency band used for successive ps $\otimes$ ps analyses. ν_{fund} is the position of the highest peak near the position expected for $\Delta\nu_0/2$, and $\nu_{harmonic}$ is the location of the highest peak near the expected position of the first harmonic. (Only the seven highest peaks over 3–200 μHz in ps $\otimes$ ps are written out in these searches; dashes imply no highest peak near the general range.)

To assess the significance of peaks in Table 14 we generated 39 independent time series realizations having similar noise distributions as the real data. We tabulated on a grid of ν_{cent} (steps of 100 μHz) vs $\Delta\nu_0/2$ (1 μHz steps at 19 μHz) how often a ps $\otimes$ ps peak (within ± 1.5 μHz of the $\Delta\nu_0/2$ grid value) from the null experiment cases exceeded that from the real data. (The comparison window of 3 μHz in the null experiment ps $\otimes$ ps spectra was chosen to be similar to the spread in, and uncertainty of, position for the ν_{fund} object peaks and is also comparable to the width of peaks. We consider this a conservative choice; obviously reducing this window would result in fewer matches from the null experiments and apparently more significant results.) All of the peaks listed in Table 14 fare well in comparison with the pure noise null experiment; on average there are only 2.1 noise realizations out of 39 yielding a peak stronger than that from the real data. Five of the peaks listed in Table 14 have no counterparts as strong from the noise realizations. Against independent realizations of scrambled data the ν_{fund} peaks appear only an average of 0.9 times out of 39 realizations each.

It is important to note that the mean noise level may vary with frequency in the real amplitude spectrum. The height of ps $\otimes$ ps (noise induced) peaks scales as the fourth power of the mean noise level (second power if analyzing power spectrum of amplitude spectrum). As an example: The mean amplitude spectrum level in a 310 μHz window centered at 1300 μHz is 12% higher than the 2.5–4.5 mHz mean tabulated in Table 13 which was used to set the null experiment realizations. Consistent with a null test we have therefore scaled ps $\otimes$ ps peaks from the noise realizations up by 24% (for amplitude spectrum) before comparison against the real data peak. If some of the power in a given window arises from a real signal this will result in an underestimate of significance.

Adopting the weaker of above results suggests that the signals shown in Table 14 are significant at the 95% level, or a 2σ result. The consistency of this signal with general expectations for stellar oscillations should further support acceptance of this as a detection. Also the coherence of the 19 μHz peak over independent (but contiguous) domains, as well as the clear presence of the harmonic provide additional confidence beyond the simple simulation results.

Comb analyses near the apparent signal peak in the

TABLE 15. ps ⊕ ps summary star No. 27.

ν_{cent}	ν_{fund}
1000	29.5
1100	29.9
1200	28.6
1300	27.7

800–1200 μHz domain are consistent with a similar 2σ level of significance in comparison against null realizations. We cannot with confidence derive a single $\Delta\nu_0$, or in the terminology of Eqs. (16) and (17), *dxnu* and *dxl*1 pair that best represents the data—several closely related values provide equally good fits. Figure 17 shows one such fit for star No. 16. We have experimented with real data analyses for star No. 16 in which the contribution from each single site was omitted in separate analysis sets. This guards against: (1) a real signal not appearing as strong as it should if the data (or times) from one site are incorrect, and (2) claiming a detection based only on strong spurious input from a single site. The general signal as shown in Table 14 is present with the omission of any single site. The signal is not strengthened by any omission. The signal was most weakened when the AAT data was omitted (star No. 16 had low noise in the AAT data and sensitivity to a splitting of 19 μHz is particularly dependent on the window function).

The results here are not strong enough to support a claim of unambiguous detection, however given our general experience based on analysis of many different simulations and null test cases, we believe the ps ⊗ ps peaks follow from stellar oscillations. But our confidence level in saying the latter is only at about the 2σ level and does not therefore serve as a firm foundation from which interpretation can be justified.

It is, however, worth pointing out that initial searches for evidence of oscillations were conducted with the $\Delta\nu_0/2=28.7$ μHz prediction in mind. Only after the analysis of the ps ⊗ ps showed evidence for mode separations of $\sim$19 μHz was Eq. (2) used to show that this was a reasonable (even more natural than Table 1 entry) value for star No. 16.

6.2 Star No. 27

This star is on the ridge line of subgiants for M67 members and has no noted radial velocity variability or photometric anomalies; theoretical predictions for its oscillation characteristics should be secure.

Table 15 details the most suggestive results from an extensive ps ⊗ ps search. At 1200 μHz a higher peak appears at 31.6 μHz splitting. The power for this star shows evidence for peaking at 1000–1200 μHz, in good agreement with expectation. The position of "harmonic" spacings as shown in Table 14 could not in general be quantified for this and other stars. The agreement between predicted separations of 28.8 and observed 27.7–29.9 μHz is excellent. Again the implied variation of $\Delta\nu_0/2$ with frequency is not

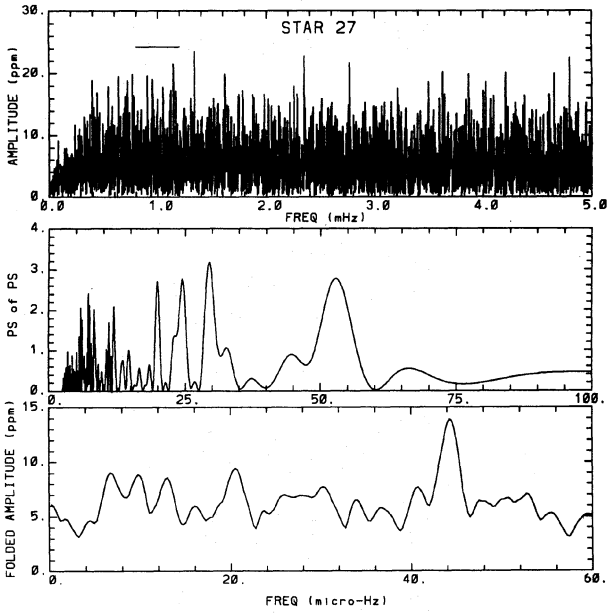

FIG. 18. Standard analysis set for real data on star No. 27 (see Fig. 13 for comparison with simulation).

unreasonable. If the ps ⊗ ps peaks are indicative of oscillations, then standard simulations suggest peak stellar oscillations of $\sim$20–23 μmag.

A comparison with noise realizations shows that in 8% of the cases on average a peak within ± 1.5 μHz is higher than the one tabulated. Only 2% of the time does as strong a signal appear in the scrambled data realizations. (For randomly selected ν_{cent},ν_{fund} pairs the noise realizations exceed stellar signals about 50% of the time as expected.)

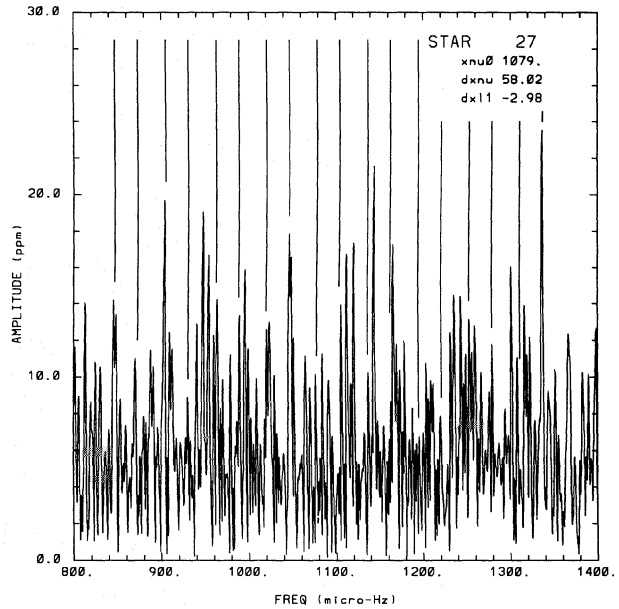

FIG. 19. Comb analysis as applied to real data for star No. 27.

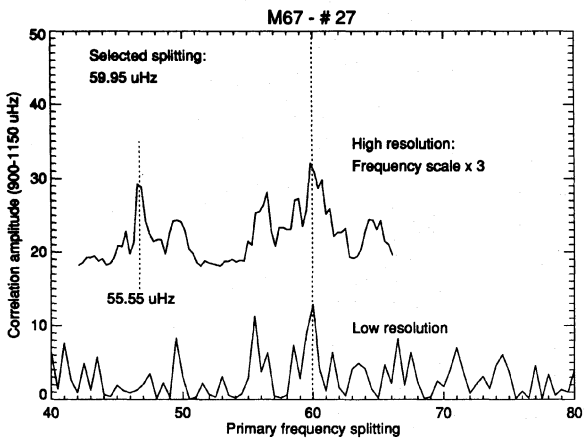

FIG. 20. Comb analysis (H. K.) as in Fig. 14, but applied to the real data time series for star No. 27.

Figure 18 shows a standard analysis set with the ps ⊗ ps window centered at 1000 μHz, while Fig. 19 illustrates a comb analysis (R.L.G.) solution.

The comb analysis used by H.K. is illustrated in Fig. 20. Our independent approaches return estimates for the most likely characteristics of underlying stellar signals that are consistent, but different in detail. Given that neither the R.L.G. nor H.K. analyses in this case allow an internal claim of a single value that best represents the possible signal in a unique way it is not surprising that our two rather different approaches return unique values *even if both are a result of the same underlying stellar signal.* The full set of comb analysis results (H.K.) will be given in Table 21 at the end of Sec. 6 along with comments concerning the general comparison of our independent analyses.

As with star No. 16 we also analyzed star No. 27 six different times with the omission of single sites in turn. The signals as shown in Table 15 were frequently less noticeable, with the omission of single sites. The signals were always present and never made stronger with the omission of single sites. This "sanity check" experiment has not turned up any surprises: The signal does not result from spurious results (no reason to expect such) at any site, nor does omission of a single site spoil the results.

6.3 Star No. 41

This star is near the M67 subgiant ridge line. Although this star is a single-lined spectroscopic binary (Mathieu *et al.* 1990), the position of the primary in the HR diagram should be reasonably precise. This star should have properties very similar to star No. 27. Table 16 shows results from a ps ⊗ ps analysis with 400 μHz wide windows.

TABLE 16. ps ⊕ ps summary star No. 41.

ν_{cent}	ν_{fund}
1200	31.0
1300	30.3

TABLE 17. ps ⊕ ps summary star No. 37.

ν_{cent}	ν_{fund}
600	21.0
700	23.9
800	23.0
900	22.5
1000	23.2
1100	24.3

Within the errors that should be assigned to the derived $\Delta\nu_0/2$ (probably ± 1.5 μHz), these results are in rough agreement with those for star No. 27. This lends some credence to interpreting the ps ⊗ ps signals as deriving from oscillations. The peak amplitudes in this case would be very nearly those suspected for star No. 27 (20–23 μmag), but the noise level is a little higher, making the ps ⊗ ps peaks less clear.

Peaks higher than those in Table 16 occur 6% of the time in noise simulations and 3% of the time with scrambled data.

6.4 Star No. 37

This star is near the ridge line for M67 subgiants. However, star No. 37 is a double-lined spectroscopic binary and although it has a well determined orbit (Mathieu *et al.* 1990), the duplicity contributes to uncertainty in the magnitude and color of the primary. Also, since the star is a very red subgiant, the model predictions have larger than usual relative uncertainties; a 20% error tolerance on the frequency separations of Table 1 is a reasonable estimate. Oscillation amplitudes are expected to peak near 650 μHz. Table 17 reviews ps ⊗ ps evidence for this star based on 200 μHz windows. If arising from stellar signals the ps ⊗ ps peaks would require amplitudes peaking at 22–27 μmag. The difference between predicted $\Delta\nu_0/2 = 17.3$ μHz and the observations near 22 μHz could be explained with a radius error of 17%, which given the general uncertainties for this star is well within the range of possibilities.

Peaks as high as those shown in Table 17 occur 6% of the time (only 3% over 700–900 μHz) in noise realizations. No equally strong peaks (out of 39 realizations) could be found in analyses of scrambled data. Again the results suggest about a 2σ significance.

6.5 Star No. 28

This star is a little to the blue of where standard evolution models pass in simulations for M67 (GB92). This star

TABLE 18. ps ⊕ ps summary star No. 28.

ν_{cent}	ν_{fund}
800	39.8
900	39.2
1000	39.4
1100	40.4
1200	40.1

TABLE 19. ps ⊕ ps summary star No. 44.

ν_{cent}	ν_{fund}
1200	32.5
1300	31.9
1400	30.7
1500	30.0

may therefore be considered a mild blue straggler; at any rate theoretical predictions are not as secure as for most of the other ensemble stars. Given the HR diagram position, oscillation amplitudes would be expected to peak near 1550 μHz. Table 18 summarizes the most suggestive results from extensive ps ⊗ ps analyses. Windows of 400 μHz were used for the ps ⊗ ps.

This star shows decent evidence for solar-like oscillations with nearly correct frequency characteristics based on the GB92 predictions. The Table 18 peaks appear as strong only 3% of the time in null experiment realizations based on noise. In realizations of the scrambled real data, the rate of equally strong peaks appearing is also 3%. This suggests a slightly better than 2σ case can be made for a detection. Amplitudes, if stellar in origin, would be in the 20–23 μmag range. Recall, however, the discussion of upper limit determinations in Sec. *5.2*—ps ⊗ ps supplied mode amplitude estimates are quite dependent upon the assumed mode distribution. Assuming a regular pattern (small offset of $l=0$ and 1 modes) with slower than assumed amplitude variation with frequency would yield amplitude estimates some 50% smaller.

6.6 Star No. 44

This is the brightest of the main-sequence stars in the ensemble. Its HR diagram position is on the MS ridge line, so models should be secure. The expected position of peak oscillations is about 1350 μHz. The ps ⊗ ps do not show particularly suggestive results for this star, but the highest peaks near the expected location of oscillations are shown in Table 19.

At $\nu_{cent}=1300$ μHz there is also a strong peak at 35.6 μHz, and at $\nu_{cent}=1500$ μHz there is a peak at 33.6 μHz. Equally strong peaks occur 14% of the time with scrambled data, but only 3% of the time with noise simulations. The peak at 1300, 35.6 μHz is never equaled in 39 noise realizations and only twice for the same number of scrambled cases. Detection significance for this star is perhaps 1.5σ.

TABLE 20. ps ⊕ ps summary star No. 48.

ν_{cent}	ν_{fund}
1200	33.1
1300	32.5
1400	33.3
1500	34.5

6.7 Star No. 48

This star is also on the main-sequence ridge line and is just a little less luminous than No. 44. The model predictions for these stars should be good; the relative differences between them (see Table 1) should be even more tightly constrained. Table 20 shows ps ⊗ ps peaks based on 400 μHz windows in the region of primary interest. This is the range over which oscillations would be expected, and the ps ⊗ ps is most suggestive with isolated peaks just in this range. At $\nu_{cent}=1200$ μHz a peak at 37.4 μHz is also strong. The $\Delta\nu_0/2\sim33.5\pm1.5$ μHz is not far from agreement with the GB92 prediction of 37.6 μHz ($\pm\sim10\%$). Equally interesting, albeit based on marginal results, is the observed difference between stars Nos. 44 and 48 which has the same sense and magnitude as the predictions. Peaks as high as those listed for star No. 48 occur only 3% of the time for either noise or scrambled data realizations. But the small differences from observations between the subgiants Nos. 27 and 41 and the main-sequence stars No. 44 and 48 is difficult to reconcile with theory.

6.8 Star No. 49

This star is well matched by main-sequence models for M67 stars. Number 49 has a slightly higher noise level than its MS neighbors (Nos. 48 and 52) as a result of a rather crowded (by brighter stars) sky position. This star does not show much evidence for solar-like oscillations, which is in agreement with expectations. As an example, Table 1 predicts a $\Delta\nu_0/2=38.9$ μHz mode separation at $\nu_{pk}=1409$ μHz for star No. 49. Examination of the Monte-Carlo simulation noise realizations over $\Delta\nu_0/2=32$ to 46 μHz and $\nu_{pk}=1100$ to 1800 μHz yields a best case of ~37 μHz at 1300 μHz, in good agreement with expectations. But the observed levels are exceeded 26% of the time by noise realizations, yielding a significance level of $\sim1\sigma$.

6.9 Star No. 52

This star is well modeled as an M67 main-sequence star. Stars Nos. 52 and 65 were not included in the AAT ensemble and thus suffer from a slightly poorer window function than the 10 stars previously discussed. However, both stars 52 and 65 are expected to have $\Delta\nu_0/2\geqslant40$ μHz, the detection of which should not be sensitive to small changes of the window function (see Fig. 12).

If, as with star No. 49, we search the Monte-Carlo simulation results within a $\pm20\%$ band of the predicted values of $\Delta\nu_0/2$ and ν_{pk} from Table 1, the best response is centered at $\Delta\nu_0/2=42$, $\nu_{cent}=1700$ μHz. The nominal significance is again at 2σ, since the real data peaks are exceeded only 5% of the time by noise peaks. To assess the true significance of this result requires asking how large a randomly chosen position in the two-dimensional space must be searched before chance allows 2σ fluctuations. By inspection this domain is about $\pm20\%$. We will further comment on overall significance of ps ⊗ ps peaks in Sec. 8.

6.10 Star No. 65

Again this star is well matched by the M67 main sequence. The position of greatest significance in the $\Delta\nu_0/2$, ν_{pk} plane within $\pm 20\%$ of predictions is at 58.5, 2400 μHz. Peaks in the noise realizations exceed the observed levels 14% of the time. Unless the oscillations on this star are at much higher amplitude than expected, we should not see any evidence of their presence.

6.11 Star No. 13

This is the bluest star (along with star No. 28) in the ensemble and, as discussed in GB92, can only be matched with some type of blue straggler model; i.e., ordinary single main-sequence members of M67 should not pass through this point in the HR diagram. For this reason models for this star are not very secure and comparisons with theory cannot be used as a good interpretive guide.

Power spectra of power spectra show isolated peaks near 40 μHz using 640 μHz bands centered at 1370 and 1690 μHz, and about 34 μHz centered at 2010 and 2330 μHz. From comparison with simulations the following can be said: If oscillations with separations of 34 μHz are imposed at 20 μmag peak amplitude over a frequency range wider than the 640 μHz ps $\otimes$ ps window, then out of 25 independent cases analyzed with a ps $\otimes$ ps the peak at 34 μHz is always the largest and easily seen. Out of 30 pure noise simulations ps $\otimes$ ps peaks never exceed 70% of the level seen in the stellar spectrum. *If* the possible signal follows from widely distributed coherent oscillations, then the amplitudes are about 14 μmags. This is, of course, model dependent: if the distribution of modes is not dense, then individual amplitudes must be higher to explain the ps $\otimes$ ps level.

Note that this was not called out in the introduction to Sec. 6 as one of the most interesting cases. The following points argue against interpreting the suggestive evidence here as indicating a detection: (1) the best suggestions of oscillations from inspection of many ps $\otimes$ ps for this star lie at or beyond the acoustic cutoff frequency; (2) implied frequency separations bear little coincidence with predictions; and (3) the implied mode distribution is not Sun-like. We do not believe that real oscillations are in evidence for star No. 13 based on these ps $\otimes$ ps analyses. The comb analysis (H.K., see summary Table 21) selects a "best-evidence" value of $\Delta\nu_0/2 = 27.2$ μHz, in good agreement with the theoretical projection given in Table 1.

6.12 Star No. 12

This star is anomalous in that its theoretical and observational time series characteristics are quite unlike those for any other star in the ensemble. Unlike all the other stars, we do not consider this red giant to be Sun-like and were not concerned (GB92) that our stellar evolution models did not extend far enough to encompass it. With a good data set for this star in hand, we will provide rough estimates for its oscillation properties and compare these with the observational results. Oscillations in star No. 12 would be expected to peak near 100 μHz [see Table 1 and Eq. (5)], a domain that is strongly suppressed by our usual time series filtering. The oscillation amplitude predictions can be taken from the interpolation formalism of Eq. (4), and suggest a lower range of about 80 μmags. The primary frequency splitting, $\Delta\nu_0/2$, may be estimated using the homology transformation $M^{1/2}R^{-3/2}$ [Eq. (2)] which predicts a value of 3.5–4.7 μHz if scaled from the subgiant entries of Table 1. The ensemble normalized, but unfiltered, time series for star No. 12 is affected more by $1/f$ noise than any of the other stars as a result of its deviant color relative to the ensemble mean. Also, as the brightest star, any residual nonlinearities would most affect the photometry for this star. For all of the other stars we produced simulations with realistic noise distributions, but given that $1/f$ noise is undoubtedly important at 100 μHz, we have not attempted such for this star. A more robust analysis for star No. 12 may be the topic of a future paper; below we will present only a preliminary discussion.

TABLE 21. Comb analyses (HK).

Star No.	$\Delta\nu_0$	l=0,1 offset	ν_{pk}	Noise	Peak Amp
12	7.78	−0.09	87.	6.09	80
13	54.41	−8.65	392.	6.30	16
16	24.16	−0.33	984.	6.45	12
27	59.64	−4.46	1024.	6.63	14
28	99.54	−14.52	1696.	7.47	18
37	27.77	−4.83	474.	7.40	16
41	61.41	−9.63	1128.	7.61	18
44	58.44	−3.29	1437.	8.15	16
48	98.45	−13.05	1230.	8.26	16
49	71.11	−9.87	1144.	9.27	18

Figure 21 shows the usual standard analysis summaries,

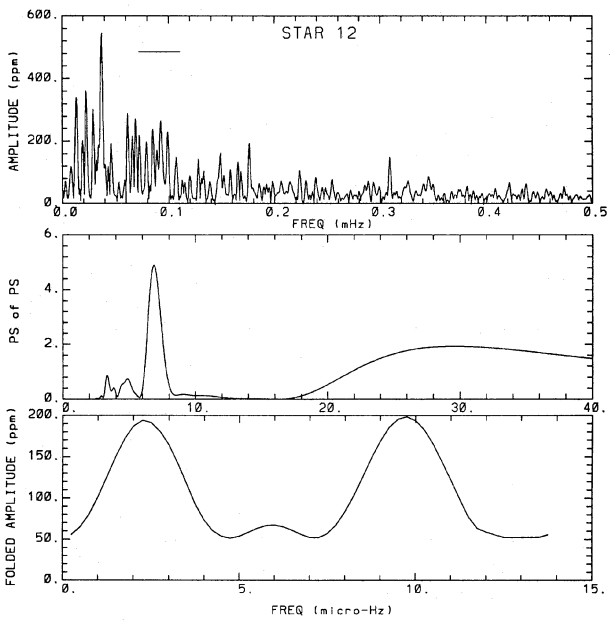

FIG. 21. Same analysis set as Fig. 13, but based on the real, unfiltered data for star No. 12. As this is the only red giant in our ensemble, interpretation of results for this star faces a number of unique difficulties discussed in the text.

but for this star only it is based on time series that have not been filtered to remove low frequencies. The ps ⊗ ps over 72–111 μHz yields a clean suggestion of repeated peaks at a separation of 6.86 ± 0.1 μHz and amplitudes of ~ 200 μmag. There is, furthermore, a tertiary peak showing up in a folded amplitude spectrum consistent with $\Delta\nu_{20} = 3.8 \pm 0.2$ μHz. These results are interesting, but given our lack of stellar evolution based eigenfrequencies for comparison and our lack of realistic noise simulations with $1/f$ noise, we will not speculate on significance.

6.13 Fainter ensemble stars

The 8 additional stars within the primary ensemble region, with magnitudes ranging from 16 to 22, have been examined for evidence of variability. The high spatial density of 12 stars of magnitude 11 to 14 in a 90″ field of view is not favorable for precision results on fainter stars. No obvious evidence was found for variability in any of the fainter stars.

It may also be worth pointing out that although we could coadd about 50 h of dark time imaging from 4 m telescopes using efficient CCDs and a broad filter, the detection threshold for faint stars was only about 23rd magnitude. This followed from our use of image scales, CCD gains, and frequent defocusing favorable to counting many tens of millions of photons per readout on the brighter stars, but quite unfavorable to the detection of faint objects. A star at 23rd magnitude typically yielded less than one ADU per integration in the peak PSF pixel.

6.14 Summary of Individual Star Results

The discussion above has emphasized results obtained by the first author. We will summarize here equally complete and careful analyses (quite independent) by H.K. and provide comparisons. Table 21 identifies the most likely signals for each of the 10 stars covered by the full ensemble.

An explanation of the columns of Table 21 follows. The $l=0$, 1 offset is defined as the average over frequencies from the comb analysis of $\nu_{n,1} - 0.5(\nu_{n+1,0} + \nu_{n,0})$. The Noise corresponds to the mean of the amplitude spectrum over 0–4 mHz (no use of CLEAN). The Peak Amp is given in ppm, and all frequencies are in μHz. The signal for star Nos. 13, 28, 41, 44, and 48 is strongest in the H.K. analysis. Confidence is at an intermediate level for Nos. 12, 27, and 37 and low for star Nos. 16 and 49.

As shown in Fig. 12 values of $\Delta\nu_0/2$ of 19 to 25 μHz are particularly sensitive to details of the window function. It may therefore follow that the application of CLEANing (as used by R.L.G.) makes the most difference for stars (Nos. 16 and 37) with expected frequency separations in this range. Further discussion of the H.K. analysis sensitivity to oscillations with these characteristics will appear in Kjeldsen *et al.* (1993).

The cases in which both independent analyses and theoretical expectations are in agreement include stars Nos. 27 and 41, although even here some secondary details like the $l=0$ and 1 offset for star No. 41 in Table 21 do not match expectations. The two analyses agree for star No. 12, but a reliable comparison with theory is not available. In most cases we could develop discussion showing agreement upon further analysis. For example, on star No. 13 $\Delta\nu_0 = 54$ μHz also appears in the R.L.G. analyses as a suggestive ps ⊗ ps peak, although evidence for its reality was not as high as for other peaks discussed. Another example is star No. 48 where the $\Delta\nu_0 = 98.5$ μHz of Table 21 and $\Delta\nu_0/2 \sim 33$ μHz of Table 20 are simple integer multiples. Other sources of "agreement" would be easy to describe in most cases.

A direct comparison of independent analyses does not inspire confidence that we have reliably detected stellar signals. This is consistent with the lack of unambiguous signals in any of the individual analyses. Further discussion of overall significance will be deferred to Sec. 8.

7. FUTURE PROSPECTS

Given that this project has provided good, but ambiguous, evidence for the existence of solar-like oscillations on a number of stars, what should the next observational steps be? We will consider three different directions to consider for asteroseismology based upon CCD ensemble photometry: (1) A network campaign similar to the current one. Are there "minor" changes to such a network that would allow greater sensitivity? (2) This project represented a state of the art, maximum effort attempt in 1992. What would a similar next generation effort, say for 1997, look like and what would its prospects be for unambiguous detections? (3) This project concentrated on the very challenging problem of solar-type stars. What other asteroseismology projects are seen as important, but not requiring 4 m class telescopes? What unique science and observational constraints will such projects face?

7.1 Simulated Sensitivity with Additional Sites

We do not intend to attempt a simple repeat of this network campaign. Although an independent repeat would be of interest to see if the marginal signals claimed here are consistently present, we do not believe a strong enough case could be made again simply to repeat the original project. Since we may have had better than average luck with weather the first time around it would be difficult to claim that a simple repeat project would necessarily attain even equal results. We are also not aware of any fundamental changes at any sites that would significantly improve their contribution to the network.

In considering possible near future campaigns for solar-like oscillation detection there are two fronts to pursue: (1) Obtaining more data, for which the gain is generally quantifiable as $N_{\rm obs}^{1/2}$. (2) Gaining greater sensitivity to modes with certain expected characteristics by providing a superior window function. We argued in Sec. *5.2* (see Fig. 12) that our realized distributed network had much better sensitivity than an equivalent single site. In reviewing our network it is clear that although we had an impressive

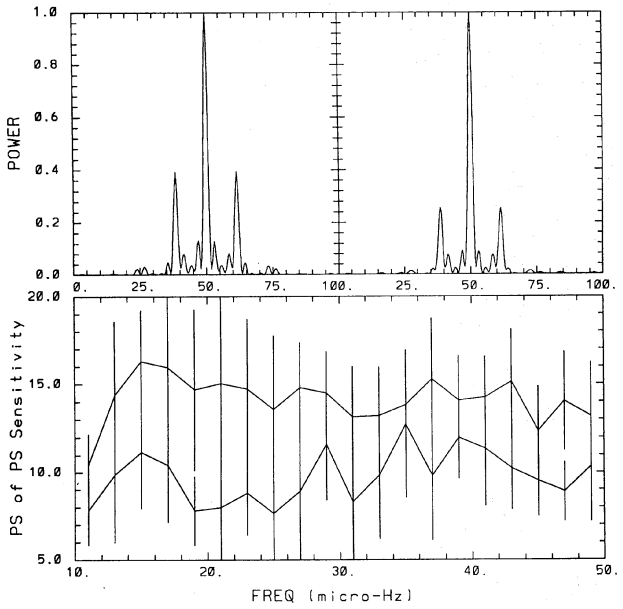

FIG. 22. Comparison of window and ps ⊗ ps response functions for the realized network campaign (lower curve) and for the augmented campaign as discussed in Sec. *7.1*. See Fig. 12 for definitions.

64% duty cycle, the data were still very heavily weighted toward the American southwest. Our eastern flank was relatively weak.

We explore here what gains would have resulted from having had the CTIO 4 m, WHT 4.2 m and the Russian 6 m telescopes as a part of the network with the five nights of 1992 January 13–17 assigned at each site. The following assumptions are made: (1) CTIO would have contributed six hour time series on each of its five nights. The combination of better observing conditions but a larger airmass for atmospheric scintillation lead to the same precisions per unit time as attained at Kitt Peak. A total of 30 h observing contributes a site sensitivity 5% poorer than the KPNO contribution, but at a unique longitude. (2) The WHT would have encountered the same weather conditions as were realized at the NOT. We make the conservative assumption that per unit elapsed time the combined WHT plus NOT contribution would have equaled that from Kitt Peak. This can be easily simulated by dropping the noise level assumed for the 20.3 h of NOT observations by a factor of 1.78. (This yields site sensitivity for star No. 16 of 47.4 ppm, see Table 2.) (3) We do not know what weather conditions held at the Russian 6 m site, but assume that the two nights of 1992 January 16–17 would have been clear. We simulate this addition by replicating the Palomar time series for the nights of January 16 and 17 shifted by the Δt of 10.6 h eastward. These three (imaginary) additions yield an increase of 64.4 h over the actually obtained 156.6. The formal network sensitivity [Eq. (7)] for star No. 16 shows a significant gain of 17% taking into account the added time at conservatively assumed precision levels. Equally or even more important is the improvement in window function. Figure 22 compares the attained (see Sec. *5.2*) and simulated window functions and ps ⊗ ps sensitivity. The improved network window combined with more data points would yield an overall sensitivity gain of 30% for $\Delta\nu_0/2 = 28$–$50\ \mu$Hz and up to 100% at $\Delta\nu_0/2 = 19\ \mu$Hz. This would drop the unambiguous sensitivity limit on star No. 16 from 28 to 14 ppm. Since this is well below the level at which we believe the star already shows evidence of oscillating, and it is well under the range expected from theory, we could anticipate clear success with a network augmented as suggested.

7.2 A Next Generation Network

Perhaps of more interest is to ask what could be done in 1997 when the leading wave of large telescopes (the 10 m Keck at Mauna Kea and the 6.5 m MMT upgrade at Mt. Hopkins) should be available. We now make the following assumptions: (1) The seven original sites, three augmentation sites from Sec. *7.1*, and the two new large telescopes all join the network campaign. (2) All allocations are for seven nights. (3) We assume a 54% rate of success with weather and equipment as with the real network campaign of 1992 January; each site will therefore average about 3.7 good nights. (4) Per unit time precision of the upgraded MMT is a factor of 1.5 better than Kitt Peak, and the Keck is a factor of 2.25 better than CFHT. (5) We do not assume any increase due to better CCDs which could well be available in 1997. This realistic simulation assumes a total allocation of 84 telescope nights yielding about 385 h of primary object time series after factoring in weather losses. This would yield a typical improvement of $\times 2.1$ over our current results (over twice the observing time with much of the increase coming from superior sites). The improvement compared to the realized network would be relatively independent of $\Delta\nu_0/2$, since the distribution would again be heavily weighted to the western U.S. The unambiguous detection limit for star No. 27 would drop from about 28 to 13 ppm, while the unambiguous sensitivity for the main-sequence objects should drop to 17 ppm. The levels at which we would see clear, quantifiable evidence of oscillations would be ~ 9 ppm for the better subgiants and ~ 12 ppm for the main-sequence stars. At such levels we would be confident of predicting quantitatively useful detections on several stars to allow a substantial test of stellar structure and evolution theory.

Can a commitment of seven nights each on the twelve largest telescopes be justified? We believe the answer is yes. For a single project this is admittedly a huge request. However, it is clear that time granted to solar-like asteroseismology proposals is more valuable if scheduled in a few massive, collaborative blocks. Viewed as a substantial fraction (one-third?) of all asteroseismology to be done over a five year period (requiring the largest telescopes), grants of seven nights at many sites no longer seem outrageous. We suggest that any next generation network campaign be developed as a broader-based community effort directly involving theorists in the preparation of justifications. We view the overall justification as a scaled-down version of what a space project would require. One substantial hindrance to pursuing a large scale network campaign is that

there is no commonly used mechanism at the potential sites for setting up such a singular event. We propose making the statement to each TAC that a similar proposal would not be resubmitted following a successful campaign for at least five years unless an argument could be made earlier supporting an expected factor of 2 gain (with a similar local resource allocation—factors of 2 gains are difficult). We envision the active collaboration of perhaps 25 astronomers with in-depth theoretical analyses supporting such a campaign. Yet the standard mechanism for telescope time applications would still only consist of a one page justification submitted a few months before the observations. A better project would follow from being able to plan to a specific block of time at some sites 2–3 years ahead of time.

Preparation for a next generation campaign should include: (1) A thorough review of potential ensemble choices given the anticipated general network. (2) A more extensive theoretical study of the selected ensemble to support detailed simulations of the oscillation detection problem and to quantify what the astrophysical payoff of the advertised campaign would be. (3) A detailed review of basic setup options, e.g., filter, f-ratios, CCDs etc. (4) A thorough analysis of how to distribute potentially available telescope time; might there be a gain to stagger some of the sites at similar longitudes to provide a longer baseline, or is it best to keep coverage as intensive as possible? (5) A broad-based effort to arrange the requisite collaboration. (6) Exploration three years ahead of time with observatory directors and telescope allocation committees (at key sites) about what proposal formats and lead times (two years suggested) could be allowed for such a community based proposal.

The European Community has vigorously supported a space based mission (PRISMA, Appourchaux 1991) for asteroseismology. If we can argue that use of the world's twelve largest telescopes for one week (a resource usage small in monetary terms compared to a spacecraft) would support a definitive result for asteroseismology of near solar-type stars, would this compromise support for a future space project? It should not. The programs proposed by PRISMA and for a next generation large telescope campaign (likely to be M67 again) are complementary. The M67 stars are too faint for PRISMA or any comparable space-based project, but the equivalent science (oscillations for a diverse, but related ensemble with a solar age as in our Table 1) to be gained also would not follow from a space experiment. PRISMA, or a similar project, should provide definitive results for the Hyades (in which Sun-like stars are unevolved) and a survey of other interesting objects. The next generation network campaign and a first generation asteroseismology satellite are complementary, not competitive.

7.3 Asteroseismology of non-Sun-like Stars

We wish to avoid giving the incorrect impression that useful asteroseismology requires such grandiose commitments as dedicated spacecraft or a week-long collaboration of the worlds largest telescopes. Already astrophysically rich results have appeared in the literature (e.g., Kurtz *et al.* 1989; Winget *et al.* 1991) based on the use of 1 m class telescopes (but comparable time and organizational complexity were nonetheless involved). There are many projects that do not require large telescopes, but would best be carried out by 0.5–1.0 m telescopes with CCDs. Two examples are: (1) δ Scuti stars. These spectral class A–F residents of the classical instability strip often show a rich set of radial and nonradial modes (Matthews 1993). Although many thousands of hours have been spent observing hundreds of δ Scuti stars, few if any cases have been fully solved. This is a field that could benefit dramatically from more studies like Kurtz *et al.* (1989), especially if directed to stars with a rich mode spectrum. (2) Red giants. There is good evidence for the existence of p-mode oscillations on Arcturus from Doppler measurements (Belmonte *et al.* 1990) acquired during a two week run with the 4.2 m WHT. Our own results for star No. 12 suggest oscillations with periods of about 3 h and amplitudes of 100 μmags for this M67 red giant. A superior observational campaign for photometric quantification of red giant oscillations would use smaller telescopes (0.5–1.0 m) with larger fields of view to contain a large set of similar stars for ensemble normalization. A campaign using 5–10 small telescopes for a two week period should provide interesting results for a large number of cluster red giants.

8. DISCUSSION

We have shown that a network campaign with 4 m telescopes using CCD ensemble photometry can reach precision levels of interest for asteroseismology of Sun-like stars. For the best cases our upper limits for an unambiguous detection are near the lower range of amplitude values predicted by theory. There is a distinct tendency for the strongest evidence for oscillations in many stars to be in agreement with theoretical expectations for the general location of greatest power and for the basic $\Delta\nu_0$ frequency separations.

For several stars (Nos. 16, 27, 28, and 37 in particular) we believe oscillations are detected. However, the significance level is only about 2σ in each case. That several stars show roughly 2σ evidence for oscillations is a cause for concern and raises a general question about how we establish the significance. We have argued that the highest peaks appearing consistently for several stars are seen only $\sim 5\%$ of the time to be as strong in null experiment comparisons. If we were to analyze any null experiment time series, selecting its highest ps $\otimes$ ps peak there would, of course, be a tendency for the same frequency to show lower amplitudes in independent realizations. As argued in the discussion for star No. 52, allowing a search for most significant peaks over a $\pm 20\%$ domain in each of $\Delta\nu_0/2$, ν_{pk} is roughly consistent with turning up a 2σ fluctuation. In no case can we claim an unambiguous detection of stellar oscillations. However, in most of the stars where a good case for oscillations is claimed the results are consistent with *a priori* expectations; in some of these cases we could claim

that the search domain was restricted to well under the $\pm 20\%$ area required to explain 2σ fluctuations. The preponderance of evidence suggests that we do see oscillations on some stars, but at too low a signal to noise to support definitive quantification.

In terms of making arguments concerning the reality of claimed signals we are in the *most awkward possible realm of sensitivity to expected signal level.* Our sensitivity relative to expected signal is just such that we would expect to often detect the signal, but not at a level sufficient to allow proof of high significance, nor to reach a stable characterization independent of analysis approach. One should not in this case expect a tidy overall picture to develop; there are valid lines of argument supporting the reality of oscillations on some of our stars, there are also valid lines of argument consistent with all having arisen from noise. If the hints of stellar oscillations we see follow from real oscillations, then a mere factor of two improvement in sensitivity would allow unambiguous detections. That stronger claims based on less real evidence are not uncommon in the literature reflects our relative conservatism, but has little direct relevance to deciding whether oscillations have indeed been detected on any of our ensemble stars.

We attained essentially the sensitivity levels quoted in applications justifying telescope time. That limiting precision photometry could be acquired at six independent sites, some of which had new equipment and/or observers inexperienced with CCD time series photometry, demonstrates how robust the technique is. We have argued that a slightly better network with more sites well away from the well represented western U.S. would allow sensitivity gains of 30%–100% for different stars in our ensemble. A next-generation campaign using larger telescopes could provide over a factor of two gain for all of the ensemble stars. Such gains would likely result in unambiguous detection of stellar oscillations for several stars and support extensive interpretation and tests of stellar structure and evolution theory.

We will provide ASCII file copies of the time series and weighting function data for the 12 ensemble stars (as shown in Figs. 10 and 11 for star No. 16) via electronic mail to anyone requesting such. Please address inquiries to R.L.G. at (Internet) gillil@stsci.edu.

We thank Ed Carder of KPNO for advice about filter options and for providing a tracing of our program filter. Paul Harding, Rich Reed, and George Jacoby provided useful advice about various aspects of the observations at KPNO. Gary DaCosta and John Barton provided advice about CCD linearity issues and specifics on the CCD used at the AAT. The staff of the NOT on La Palma is thanked for their help before and during the observations, especially, Toomas Erm, Paco Armas, Frank G. Jensen, and the director Arne Ardeberg. H.K. thanks Andrew Jones, Michael Andersen, and Tim Bedding for discussion and inspiration related to power spectrum analysis, Jørgen Christensen-Dalsgaard for discussions concerning the theoretical aspects of the analysis, and Aarhus University, The Carlsberg Foundation, The Danish Board for Astronomical Research, and the European Southern Observatory for financial support during the project. J. A. B. expresses gratitude for hospitality during a 1992 visit to ST ScI. Robert Noyes, Peter Nisenson, Nick Suntzeff, and Steven Vogt are thanked for their efforts in applying for or considering the possible contributions of other telescopes during the planning period for the network campaign. R.L.G. acknowledges support from the Directors Discretionary Research Fund at St ScI.

REFERENCES

Appourchaux, T., *et al.* 1991, Report on the Assessment Study, Probing Rotation and Interior of Stars: Microvariability and Activity, ESA, SCI(91) 5
Belmonte, J. A., Jones, A. R., Pallé, P. L., & Roca Cortés, T. 1990, ApJ, 358, 595
Belmonte, J. A., Pérez Hernández, F., & Roca Cortés, T. 1990, A&A, 231, 383
Brown, T. M. 1991, in Frontiers of Stellar Evolution, edited by D. L. Lambert (Astronomical Society of the Pacific, San Francisco), p. 139
Chevalier, C., & Ilovaisky, S. A. 1991, A&AS, 90, 225
Christensen-Dalsgaard, J. 1988, in Advances in Helio- and Asteroseismology, edited by J. Christensen-Dalsgaard and S. Frandsen (Reidel, Dordrecht), p. 3
Christensen-Dalsgaard, J., & Frandsen, S. 1983, Solar Phys., 82, 469
Cox, J. P. 1980, Theory of Stellar Pulsation (Princeton University Press, Princeton)
Demarque, P., Green, E. M., & Guenther, D. B. 1992, AJ, 103, 151
Eggen, O. J. 1963, ApJ, 138, 356
Eggen, O. J., & Sandage, A. R. 1964, ApJ, 140, 130
Fagerholm, E. 1906, Inaugural dissertation, Uppsala
Fröhlich, C., 1991, private communication
Gilliland R. L., & Brown, T. M. 1988, PASP, 100, 628 (GB88)
Gilliland, R. L., & Brown, T. M. 1992, PASP, 104, 582 (GB92)
Gilliland, R. L., *et al.* 1991, AJ, 101, 541 (G91)
Girard, T. M., Grundy, W. M., López, C. E., & van Altena, W. F. 1989, AJ, 98, 227
Gough, D. O. 1987, Nature, 326, 257
Gough, D. O., & Toomre, J. 1991, ARA&A, 29, 627
Hobbs, L. M., & Thorburn, J. A. 1991, AJ, 102, 1070
Howell, S. B. 1989, PASP, 101, 616
Jiménez, A., Álvarez, M., Andersen, N. B., Domingo, V., Jones, A., Pallé, P. L., & Roca Cortés, T. 1990, Solar Phys., 126, 1
Kjeldsen, H., & Frandsen, S. 1992, PASP, 104, 413 (KF92)
Kjeldsen, H. 1993a, Doctoral dissertation, Aarhus
Kjeldsen, H. 1993b, in Proceedings of the 5th ESO/ST-ECF Data Analysis Workshop, Garching (in press)
Kjeldsen, H., *et al.* 1993, in preparation
Kurtz, D. W., *et al.* 1989, MNRAS, 240, 881
Lasker, B. M., Sturch, C. R., McLean, B. J., Russell, J. L., Jenkner, H., & Shara, M. M. 1990, AJ, 99, 2019
Libbrecht, K. G., & Woodard, M. F. 1991, Science, 253, 152
Mangeney, A., Däppen, W., Praderie, F., & Belmonte, J. A. 1991, A&A, 244, 351
Mathieu, R. D., & Latham, D. W. 1986, AJ, 92, 1364
Mathieu, R. D., Latham, D. W., & Griffin, R. F. 1990, AJ, 100, 1859
Matthews, J. M. 1993, in GONG 1992: Seismic Investigation of the Sun and Stars, edited by T. M. Brown (Astronomical Society of the Pacific, San Francisco), p. 303

McCarthy, J. K. 1992, in Annual Report of the Palomar Observatory, edited by G. Neugebauer
Morgan, J. G., & Eggleton, P. P. 1978, MNRAS, 182, 219
Nissen, P. E., Twarog, B. A., & Crawford, D. L. 1987, AJ, 93, 634
Press, W. H., Teukolsky, S. A., Vetterling, W. T., & Flannery, B. P. 1992, Numerical Recipes (Cambridge University Press, Cambridge)
Pritchet, C. J., & Glaspey, J. W. 1991, ApJ, 373, 105
Roberts, D. H., Lehar, J., & Dreher, J. W. 1987, AJ, 93, 968
Robinson, R. D., Sadler, E. M., Barton, J. R., & Straede, J. O. 1989, A Users Guide to CCD Detectors at the AAT, AAO UM 17.1
Sanders, W. L. 1977, A&AS, 27, 89
Scargle, J. D. 1982, ApJ, 263, 835
Stetson, P. B. 1987, PASP, 99, 191
Stetson, P. B. 1989, AJ, 97, 1360
Stetson, P. B. 1990, PASP, 102, 932
Stetson, P. B. 1991, private communication
Tassoul, M. 1980, ApJS, 43, 469
Toutain, T., & Fröhlich, C. 1992, A&A, 257, 287
Ulrich, R. K. 1986, ApJ, 306, L37
Vandakurov, Y. V. 1968, Sov. Astron.–AJ, 11, 630
Winget, D. E., *et al.* 1991, ApJ, 378, 326
Woodard, M. F., & Hudson, H. S. 1983, Nature, 305, 589
Young, A. T. 1967, AJ, 72, 747
Young, A. T. 1974, in Methods of Experimental Physics, 12, Part A, edited by N. Carleton (Academic, New York)
Young, A. T. 1992, private communication